

Wi-Fruit: See Through Fruits with Smart Devices

YUTONG LIU, Shanghai Jiao Tong University, China

LANDU JIANG, Shenzhen University, China

LINGHE KONG, Shanghai Jiao Tong University, China

QIAO XIANG, Xiamen University, China

XUE LIU, McGill University, Canada

GUIHAI CHEN, Shanghai Jiao Tong University, China

People usually assess fruit qualities from external features such as color, shape, size, and texture. However, it is quite common that we select fruits with perfect appearances but rotten inside, especially for fruits with thick pericarps. Thus the accurate measurement is desirable to evaluate the internal conditions of fruits. As two key features of fruit internal qualities, existing methods on measuring fruit moisture and soluble solid contents (SSC) are either destructive or costly, limiting their adoption in daily life. In this paper, we propose *Wi-Fruit*, a non-destructive and low-cost fruit moisture and SSC measurement system leveraging Wi-Fi channel state information (CSI). First, to cope with the fruit structure dependency challenge, we propose a double-quotient model to pre-process CSI on adjacent antennas. Second, to address the fruit size and type dependency challenges, a lightweight artificial neural network (ANN) model with visual information fusion is proposed for fruit moisture and SSC estimations. Extensive evaluations are conducted on 6 types of fruits with both thick (*i.e.*, watermelon and grapefruit) and thin pericarps (*i.e.*, dragon fruit, apple, pear, and orange) over a month in either an empty laboratory room or a library with massive books. Results demonstrate that *Wi-Fruit* achieves an acceptable estimation accuracy (RMSE=0.319). It is independent of various fruit structures, sizes, and types, while also robust to time and environmental changes. The fruit internal sensing capabilities of *Wi-Fruit* can help fruit saving and safety in both pre-harvest and post-harvest applications.

CCS Concepts: • **Human-centered computing** → **Ubiquitous and mobile computing**; **Ubiquitous and mobile computing systems and tools**.

Additional Key Words and Phrases: Fruit Sensing, Wi-Fi, CSI, Moisture, Soluble Solid Content, Signal Processing, Image Processing, ANN

ACM Reference Format:

Yutong Liu, Landu Jiang, Linghe Kong, Qiao Xiang, Xue Liu, and Guihai Chen. 2021. Wi-Fruit: See Through Fruits with Smart Devices. *Proc. ACM Interact. Mob. Wearable Ubiquitous Technol.* 5, 4, Article 169 (December 2021), 29 pages. <https://doi.org/10.1145/3494971>

1 INTRODUCTION

The United Nations (UN) General Assembly designated 2021 the international year of fruits and vegetables, indicating the rising awareness on the important roles of fruits and vegetables in human health as well as the UN sustainable development goals [1]. According to a report by the Food and Agriculture Organization (FAO) of the

Authors' addresses: Yutong Liu, isabelleliu@sjtu.edu.cn, Shanghai Jiao Tong University, China; Landu Jiang, landu.jiang@szu.edu.cn, Shenzhen University, China; Linghe Kong, linghe.kong@sjtu.edu.cn, Shanghai Jiao Tong University, China; Qiao Xiang, qiaoxiang@xmu.edu.cn, Xiamen University, China; Xue Liu, xueliu@cs.mcgill.ca, McGill University, Canada; Guihai Chen, gchen@cs.sjtu.edu.cn, Shanghai Jiao Tong University, China.

Permission to make digital or hard copies of all or part of this work for personal or classroom use is granted without fee provided that copies are not made or distributed for profit or commercial advantage and that copies bear this notice and the full citation on the first page. Copyrights for components of this work owned by others than ACM must be honored. Abstracting with credit is permitted. To copy otherwise, or republish, to post on servers or to redistribute to lists, requires prior specific permission and/or a fee. Request permissions from permissions@acm.org.

© 2021 Association for Computing Machinery.

2474-9567/2021/12-ART169 \$15.00

<https://doi.org/10.1145/3494971>

UN, 1.3 billion tons of food (a third of global production) had been wasted worldwide in 2020, which is enough to feed 3 billion people [2]. Crops like fruits and vegetables have the highest post-harvest wastage rates of any food [3]. Thus, the evaluation of fruit quality has significant value on combating fruit waste while meeting the increasing quality demand of consumers.

Fruit quality evaluations rely on both external and internal factors. External factors of fruits such as color, shape, size, and the absence of surface bruise, can be inspected by human eyes [4], which are usually used to judge the quality of fruits in daily life. Some vision-based fruit sorting systems [5–8] also take these external features for fruit freshness classification. However, it is biased to judge fruit quality only from external factors, as it is quite common to select a watermelon with the normal outside but rotten inside. As two key internal features, the measurements on fruit moisture and soluble solid content (SSC) levels can help to eliminate such bias. The widely used commodity off-the-shelf (COTS) analyzers perform in a destructive manner. *Penetrometer* [9, 10] and *vacuum oven* [11] measure the water contents of fruits by probe insertion and heat drying. *Refractometers* [12, 13] calculate sugar levels from the light refraction on juice samples. *Spectrometers* [14], on the contrary, non-destructively and comprehensively measure these two factors from different absorption, reflection, and scatter degrees of near-infrared (NIR) signals emitted to fruit tissues. The professional editions of spectrometer [15] can provide relatively accurate measurements (± 1 Brix ($^{\circ}\text{Bx}$) on SSC and $\pm 1.7\%$ on moisture) [16, 17] but require high costs (around 100k US dollars) and controlled laboratory settings [18]. Although its portable version is cheaper (still cost 9000 US dollars) [19], it has an unsatisfactory accuracy on fruits with thick pericarps, such as watermelons and grapefruits.

To avoid destructive and high-cost fruit internal measurements, efforts have been made on radio frequency (RF)-based fruit sensing. It leverages the phenomenon that RF waves suffer from different velocity loss and propagation attenuation when penetrating through fruits with different moisture and SSC levels. Ren et al. [20] proposed a machine learning (ML) driven fruit moisture classification system with 0.75-1.1 terahertz (THz) waves. But its implementation requires a specialized platform like Swissto12 MCK, limiting its adoption in daily usage. Tan et al. [21] built fruit ripeness profiles over 600MHz bandwidth of commodity Wi-Fi at 5GHz, while they failed to provide fine-grained biological feature measurements such as moisture and SSC values of fruits.

In this paper, we propose *Wi-Fruit*, a non-destructive and low-cost fruit moisture and SSC measurement system leveraging Wi-Fi channel state information (CSI). *Wi-Fruit* targets various types of fruits with either thick (*i.e.*, watermelon and grapefruit) or thin pericarps (*i.e.*, dragon fruit, apple, pear, and orange). Specifically, fruit moisture and SSC levels are closely related to the permittivity and electrical conductivity (EC) of fruit pulps, resulting in amplitude and phase changes when Wi-Fi signals penetrate through fruits. Taking this fact, *Wi-Fruit* collects the CSI of the target fruit when it is deployed statically on the Line of Sight (LoS) link between Wi-Fi transceivers. It measures the CSI changes of penetrated Wi-Fi signals and then maps them to fine-grained biological properties (*i.e.*, fruit moisture and SSC levels).

Although recent advances have been made on RF-based material sensing [21–30], the practical implementation of *Wi-Fruit* entails substantial challenges:

- (1) **Fruit structure dependency:** The different chemical components of fruit pericarp and pip result in differentiated impacts on penetrated signals compared with fruit pulp. And the thicknesses of fruit pericarp and pip are unknown under non-destructive sensing, which would introduce errors in estimation.
- (2) **Fruit size dependency:** The phase and amplitude changes of penetrated signals depend not only on fruit moisture and SSC levels but also on target sizes, which correlate with different lengths of transmission paths through fruits.
- (3) **Fruit type dependency:** The accurate biological feature measurements require the awareness of fruit types, which are corresponding to specific electrical-biological mapping relations.

First, to cope with the fruit structure dependency challenge, we propose a double-quotient model to pre-process raw CSI readings. This model goes beyond the commonly used CSI quotient model [31]. It combines two different CSI quotients, one is the CSI quotient with or without the target object, and the other is the CSI quotient between two adjacent antennas. Assuming that path differences happen in fruit pericarps and pips are the same for adjacent antennas, this model can eliminate the effect of fruit structure dependency while achieving signal denoising. To further reduce the multi-path impact, we select the processed amplitude ratio and phase difference values with the lowest package variances and average them for further biological feature estimations. Second, to address the fruit size and type dependency challenges, we propose an information fusion-based estimation module in *Wi-Fruit*. This module aims to accurately determine fruit moisture and SSC values with sensing and visual information fusion. The sensing information is the averaged amplitude and phase differences acquired from the previous double-quotient model, and the visual information includes fruit size, shape, and type acquired from image processing algorithms. They are together input into a 3-layer lightweight ANN model to obtain the final fruit moisture and SSC estimations, which provides the highest estimation accuracy among classic lightweight non-linear regression models.

The main contributions of this paper are summarized as follows:

- (1) We propose a non-destructive and low-cost fruit moisture and SSC measurement system with commodity Wi-Fi. To the best of our knowledge, our approach is the first one that considers fruit structure, size, and type dependencies which can provide fine-grained fruit internal feature measurements. This system can be easily deployed in realistic scenarios and is helpful for both pre-harvest and post-harvest applications of fruits.
- (2) We propose a double-quotient model for raw CSI pre-processing between adjacent antennas. The one model solves two pin spots in fruit internal sensing, which can remove fruit structure dependency and denoise received signals as well. It enables the compatibility of the *Wi-Fruit* to various types of fruits and different environments.
- (3) We design an information fusion-based estimation method with a lightweight ANN for the accurate determination of fruit moisture and SSC levels. The visual information assists to remove fruit size and type dependency while fusing with sensing information, thus obtaining higher estimation accuracy than ones with individual aspects. The lightweight ANN, in addition, enables the compatibility of *Wi-Fruit* with commodity smart devices.
- (4) We conduct extensive experiments and case studies using various fruits of different structures, sizes, and types to evaluate the performance of *Wi-Fruit*. These evaluations not only present the efficiency and robustness of *Wi-Fruit* but also reveal the in-depth relationships between external and internal fruit features from the perspectives of signal science and biology.

The rest of the paper is organized as follows. Section 2 introduces backgrounds and motivations of *Wi-Fruit* on fruit moisture and SSC measurements. Section 3 and 4 respectively propose detailed designs and implementation details of *Wi-Fruit*. Section 5 presents evaluations and case studies on real-collected fruit data. Section 6 reviews the related work in non-destructive fruit sensing. Section 7 discusses how this work can be extended in the future and Section 8 finally concludes the paper.

2 BACKGROUND & MOTIVATIONS

In this section, we first present several potential scenarios on measuring fruit moisture and SSC levels in daily life, and then introduce existing COTS devices and research attempts on such measurements. For a better understanding of readers, we further show the RF-based fruit sensing theories. The substantial challenges for Wi-Fi-based fruit moisture and SSC measurements are also analyzed, which motivate the design of *Wi-Fruit*.

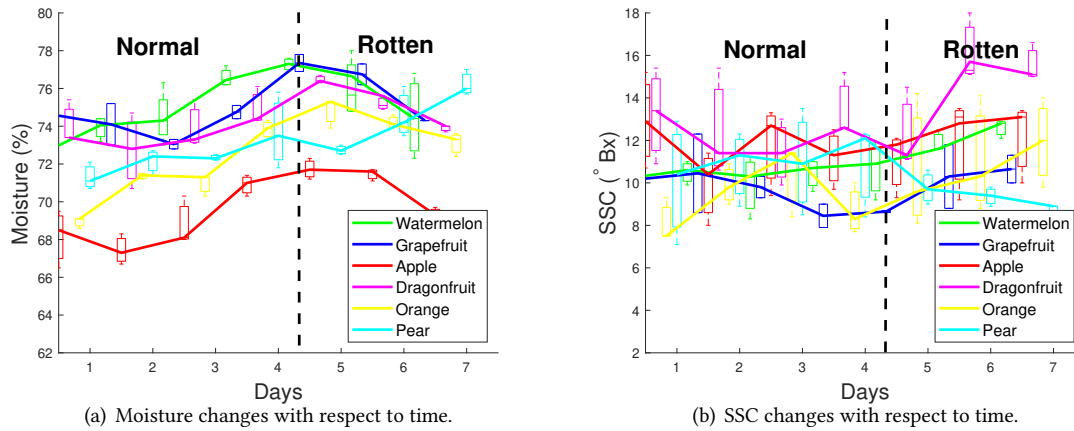


Fig. 1. Moisture and SSC observations with respect to time.

2.1 Fruit Moisture and SSC Measurements: Potential Scenarios

The moisture and SSC levels are two key features to describe the internal quality of fruits. These two features may be used in the following practical scenarios:

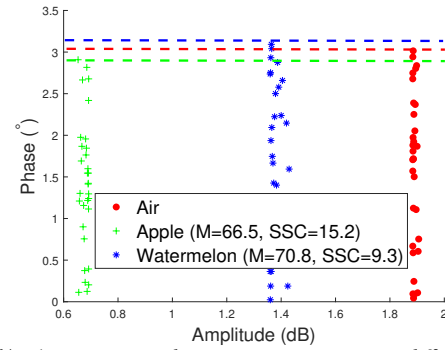
- Pick “yummy” fruits in shops.** Most of the fruit selection behaviors in daily life depend on the experience of customers. They may judge the quality of fruit from its color, shape, firmness, weight, skin characteristics, and even smell, that is, most judgments are based on external features of fruits. These judgments are biased because it is quite common to pick fruits with the beautiful outside but tasteless inside. The accurate sensing of the internal qualities of fruits can make the selection of fruits no longer a lottery-like behavior. For this application scenario, customers would like to get fast feedback with minimum effort. So, the measurements of fruit moisture and SSC levels are required to be non-destructive, lightweight, and convenient to be deployed.
- Distinguish rotten fruits and protect our health.** The rotten pulps are more dangerous than tasteless pulps as they may threaten our health. In order to extend the freshness of the cut fruit, we may cover it with plastic wrap and store it in the refrigerator. However, the rot of these protected fruits is not easy to show up in a short time. Observed from our collected data, there are rotten thresholds for moisture and SSC levels on each fruit type. As shown in Fig. 1, for example, the moisture of watermelon above 77 and the SSC above 10 imply the rot of watermelons. Once we acquire the exact values of moisture and SSC, we can judge the fruit status with the comparison of these thresholds.
- Provide a coarse storage suggestion on household fruits.** Further in Fig. 1, both moisture and SSC levels show monotonic change after the 4th day when the fruit is about to rot. (Except pear, other fruits are monotonically decreasing on moisture and increasing on SSC after they rot.) The slope for either moisture and SSC with respect to time can be estimated for each fruit type, which would be the reference to calculate the left days before the fruit rots with the consideration of its present moisture and SSC values. So a coarse storage suggestion can be given to reduce the household fruit waste.

2.2 Fruit Moisture and SSC Measurements: Existing Methods

Existing COTS devices for measuring fruit moisture and SSC levels are summarized in Table. 1 and Fig. 2 (a). The portable penetrometers [9, 10] reads the voltage difference between two probes inserting into fruit tissues

Manner	Destructive		Non-destructive
	Penetrometer & Vacuum Oven	Refractometer	Spectrometer
Portable	 US\$400	 US\$100	 US\$9000
Dedicated	 US\$3500	 US\$2500	 US\$100K

(a) The classification and price of COTS fruit sensing devices.



(b) The Wi-Fi signal transmission attenuates differently when penetrating through fruits with various moisture (M) and SSC levels than in the air.

Fig. 2. Fruit sensing motivations.

for moisture estimation. The vacuum oven [11] leveraged in laboratories provides more accurate water content evaluations through drying fruit samples under restricted conditions. Refractometer [12, 13] measures SSC via light refraction on juice samples. However, all these devices have a limited adoption range as they can only perceive a single internal feature in a destructive manner. On the contrary, spectrometers [32, 33] become a promising selection for internal fruit quality assessment which can non-destructively provide both moisture and SSC measurements. But as surveyed in Table. 1, these devices require relatively high cost (9k-100k US dollars), making them infeasible for daily use.

As observed from Fig. 2 (b), RF waves penetrating through fruits suffer from different transmission attenuation than in the air with respect to its moisture and SSC levels. Thus, it is feasible to measure fruit moisture and SSC with RF signal processing. Ren et al. [20] and Tan et al. [21] have explored this feasibility by building fruit ripeness profiles over 0.75-1.1 THz or 5GHz RF spectrum, while they did not provide fine-grained internal feature analysis with low costs. In this paper, we utilize commodity Wi-Fi for a non-destructive and low-cost fruit moisture and SSC measurements, named as *Wi-Fruit*. To the best of our knowledge, *Wi-Fruit* is the first attempt on fine-grained fruit moisture and SSC measurements with commodity Wi-Fi signals. In the following subsections, we will introduce the general RF-based fruit sensing theories and substantial challenges when Wi-Fi-based sensing comes to the fruit scenario.

2.3 RF-based Fruit Moisture and SSC Measurements: Fundamentals

RF-based internal feature sensing relies on the fact that *RF waves suffer from velocity loss and transmission attenuation through targets than in the air due to their different permittivity and EC values.*

2.3.1 Electrical Properties. Apparent permittivity and EC are two main electrical properties leveraged in existing RF-based sensing techniques [22].

- (1) *Permittivity* ϵ^* is a complex value represented as $\epsilon^* = \epsilon' + j\epsilon''$, where $j = \sqrt{-1}$. Its real component ϵ' measures the ability of the material to store electromagnetic energy, and the imaginary component ϵ'' measures electrical energy loss. The *relative permittivity* ϵ_r^* is calculated by dividing ϵ^* with the free space permittivity $\epsilon_0 = 8.854 \times 10^{-12} F/m$, which is represented as:

$$\epsilon_r^* = \frac{\epsilon^*}{\epsilon_0} = \frac{\epsilon'}{\epsilon_0} + j \frac{\epsilon''}{\epsilon_0} = \epsilon'_r + j\epsilon''_r. \quad (1)$$

Table 1. The COTS devices for fruit internal factor measurements. [Ref.=reference, M=Moisture, D=destructive, ND=non-destructive, the unit of price: US\$]

Class	Example	Ref.	Techniques	Factor	Manner	Price	Accuracy	Scheme
Penetrometer	Jacks JK-100R	[9, 10]	Voltage difference between inserted probes	M	D	400	±0.1%	Portable
Vacuum oven	Yamato ADP-31	[11]	Weight loss after infrared heating	M	D	3500	±0.01%	Dedicated
Refractometer	Mileseey SM20	[12]	Light refraction on juice samples	SSC	D	100	±0.2°Bx	Portable
	Atago Pallete PR	[13]				2500	±0.1°Bx	Dedicated
Spectrometer	Felix F-750	[19]	Near-infrared spectrum analysis	M +SSC	ND	9000	M: ±4.5% SSC: ±2.7°Bx	Portable
	ASD LabSpec 4	[15, 16]				100K	M: ±1.7% SSC: ±1°Bx	Dedicated

The *apparent permittivity* ϵ_a is the permittivity measured in situ at frequency f . It is also related to the EC θ , given as:

$$\begin{aligned}\epsilon_a &= \frac{\epsilon_r'}{2} \left[\sqrt{1 + \tan^2 \delta} + 1 \right] \\ &= \frac{\epsilon_r'}{2} \left[\sqrt{1 + \frac{\epsilon_r'' + \frac{\theta}{2\pi f \epsilon_0}}{\epsilon_r'} + 1} \right].\end{aligned}\quad (2)$$

(2) The *apparent EC* θ_a is the EC measured in situ at frequency f . It is represented by both the EC θ and the imaginary part of permittivity ϵ_r'' , as they are both related to energy loss. So it is denoted as:

$$\theta_a = \theta + 2\pi f \epsilon_0 \epsilon_r''.\quad (3)$$

2.3.2 Penetrated Wave Analysis. These electrical properties can be obtained by analyzing phase and amplitude changes of waveform penetrating through target materials. The received waveform after penetrating through the distance d can be modelled as: $R(d) = Ae^{-\alpha} \cdot e^{-j\beta d}$. The amplitude attenuation factor α and the phase change factor β in this function can be represented by the above mentioned permittivity and EC as:

$$\alpha = \frac{2\pi f}{c} \sqrt{\frac{\epsilon_r'}{2} \left[\sqrt{1 + \tan^2 \delta} - 1 \right]},\quad (4)$$

$$\begin{aligned}\beta &= \frac{2\pi f}{c} \sqrt{\frac{\epsilon_r'}{2} \left[\sqrt{1 + \tan^2 \delta} + 1 \right]} \\ &= \frac{2\pi f}{c} \cdot \sqrt{\epsilon_a}.\end{aligned}\quad (5)$$

Thus, electrical properties of target fruits can be estimated from amplitude and phase changes when signal penetrating through them, so as to be used for further biological feature measurements.

2.3.3 Biological Properties. Among various fruit biological properties, we focus on measuring fruit moisture and SSC, not only because they are strongly related to electrical properties of penetrated RF waves, but also because they are two of the most representative properties for fruit internal quality assessment [34]. Here we denote *fruit moisture* as M , demonstrating water contents in fruit tissues. It is related to the apparent permittivity

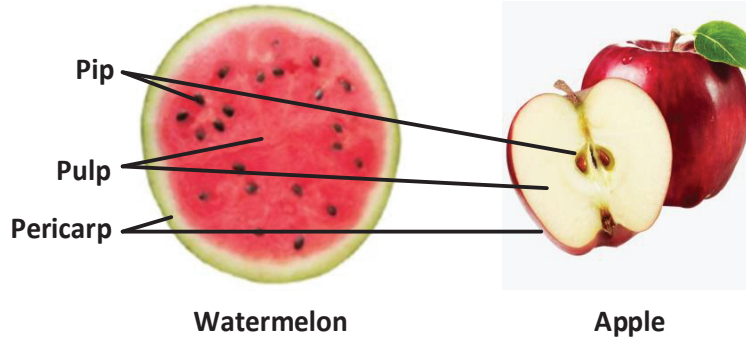


Fig. 3. Fruit composition.

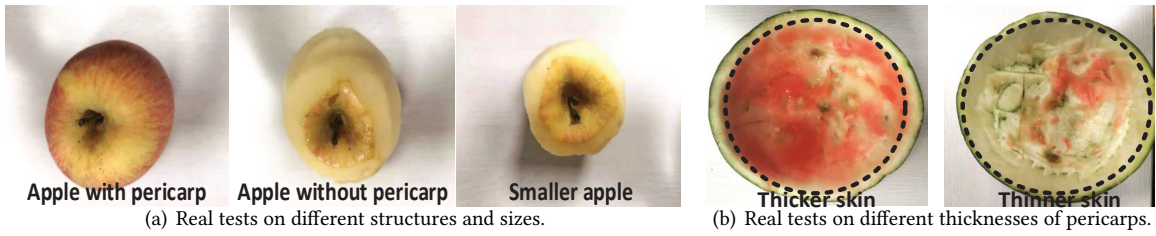


Fig. 4. Fruit structure and size dependency related real tests.

ϵ_a [35], given as:

$$M(\%) = 0.118\sqrt{\epsilon_a} - 0.117. \quad (6)$$

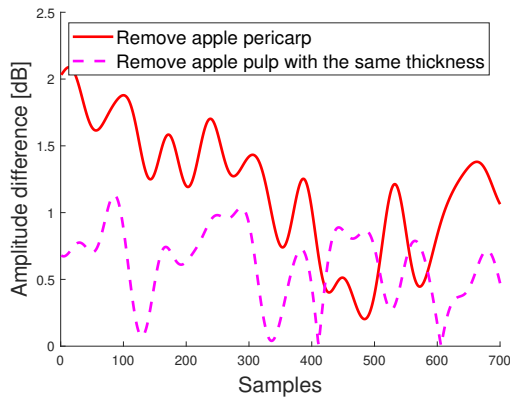
And the *fruit SSC* is denoted as S , composed mainly by sugars thus measuring fruit sweetness. The mapping relation from the apparent EC θ_a to S is presented as [36]:

$$S(^{\circ}Bx) = 640 \times \theta_a. \quad (7)$$

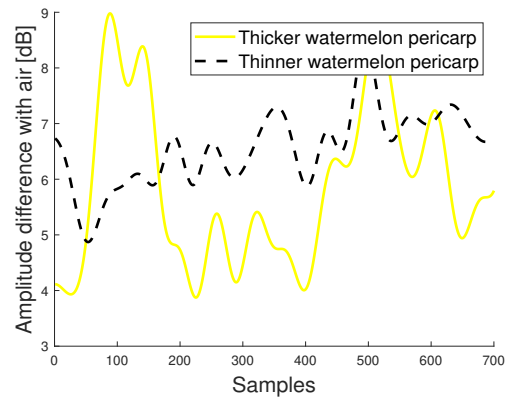
2.4 Wi-Fi-based Fruit Moisture and SSC Measurements: Motivations

Various attempts have been made on RF-based internal sensing, such as with RFID [24–26], ultra-wideband (UWB) [27], or 60GHz radars [28, 29]. Compared with them, Wi-Fi-based sensing [22, 23, 30, 37] is more convenient with lower cost due to the wide deployment of Wi-Fi modules either on smart devices or in our living environment. So it becomes a promising solution on non-destructive and low-cost fruit moisture and SSC measurements. However, accurate measurements entail a number of substantial challenges:

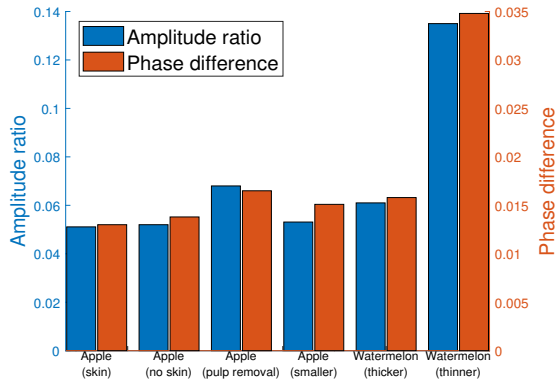
- (1) **Fruit structure dependency:** Sensing targets in recent work [22, 23, 27] are deployed in specially designed size-known containers (such as the polypropylene beaker used for liquid sensing [23] or waterproof boxes in soil sensing [22]). The container impact can be simply eliminated in these problems and researchers can concentrate on penetration attenuation caused by the contained material. In non-destructive fruit sensing, we cannot break the original structures of fruits, which means the impact on penetrated signals caused by each composition of fruits should be discussed. As illustrated in Fig. 3, most fruits consist of a pericarp, pulp, and pip. We conduct several real tests on fruits holding different compositions to explore the fruit structure impact on penetrated signals as shown in Fig. 4. We retrieve the CSI of received signals with Intel 5300 Wi-Fi card [38] deployed on a laptop. To avoid the random phase jump problem when collecting CSI with this tool



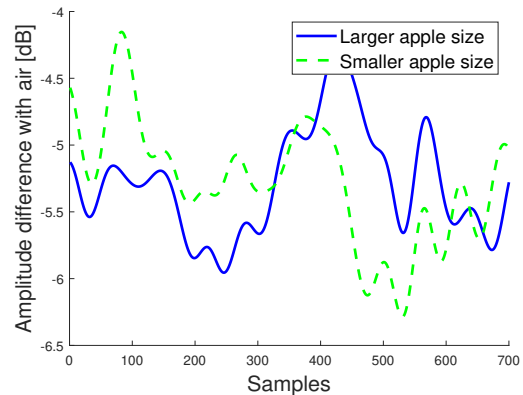
(a) The amplitude differences between apple pericarp and pulp with the same thickness.



(b) The amplitude differences between thicker and thinner watermelon pericarps.



(c) The amplitude ratios and phase differences under all discussed circumstances (full apple, apple without skin, apple with same thick pulp removal, smaller apple with same moisture and SSC, thicker watermelon pericarp, and thinner watermelon pericarp).



(d) The amplitude difference between larger and smaller apples with the same moisture and SSC levels.

Fig. 5. Fruit structure and size dependency related real test results.

at 2.4GHz frequency [39], we select a 5GHz Wi-Fi spectrum for measurements in this paper. Analysis results based on these real tests are summarized in Fig. 5. Accordingly, we get the following observations:

- (a) **Different CSI impacts for pericarps and pulps:** Fig. 5 (a) corresponds to real tests on the former two figures in Fig. 4 (a), where the red solid line represents the amplitude difference before and after removing apple pericarp, and the pink dot line represents the amplitude difference from pericarp removal to pulp removal with the same thickness. It can be seen that the amplitude changes caused by the pericarp and pulp with the same thickness are different, due to their different chemical compositions. As we mainly care about the moisture and SSC levels of fruit pulps, the impacts from other fruit compositions should be carefully eliminated.
- (b) **Different CSI impacts for pericarps with different thicknesses:** Real tests in Fig. 4 (b) are conducted on the same watermelon with only skin left. The amplitude results shown in Fig. 5 (b) indicate that the

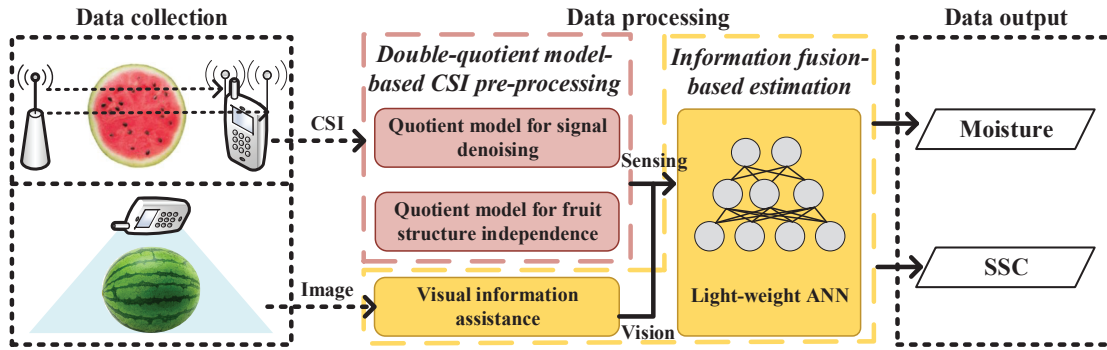


Fig. 6. The system overview of *Wi-Fruit*.

signal attenuation degrees are quite different with respect to different thicknesses of pericarps under the same fruit size.

- (c) **Sensitive CSI impacts for fruits with thick pericarps:** When summarizing all above real test results in Fig. 5 (c), it can be observed that the signal attenuation is more sensitive to changes in the structure of fruits with thick pericarps like watermelons.

Observed from these real tests, pericarps of fruits perform as a natural “container” for our sensing targets (fruit pulp). Therefore, it becomes a challenging part that the size of this “container” is unknown when measuring the moisture and SSC levels of fruit pulps non-destructively.

- (2) **Fruit size dependency:** After eliminating the fruit structure dependency, the remaining phase and amplitude changes of retrieved CSI are related to biological features of fruit pulps. However, these changes depend not only on fruit moisture and SSC levels but also on target sizes, which correlated with different penetration path lengths through fruits for Wi-Fi signals. Real tests shown in the latter two figures of Fig. 4 (a) are conducted on the same apple without pericarps, which is sliced from the bigger size to a smaller one. The evaluation results in Fig. 5 (d) demonstrate that the signal attenuation would be different due to the size impact when the moisture and SSC levels keep the same. So to acquire accurate fruit moisture and SSC estimation results, we should further eliminate the fruit size dependency.
- (3) **Fruit type dependency:** Different fruit types relate to different electrical-biological mapping functions. Specifically, the formats and parameters in function 6 and 7 should be fine-tuned for different fruit types.

3 SYSTEM DESIGN

In order to provide fine-grained internal fruit evaluation, we design a non-destructive and low-cost fruit moisture and SSC measurement system mainly depending on commodity Wi-Fi, named as *Wi-Fruit*. In this section, we present the system overview of *Wi-Fruit* and its detailed design.

3.1 The System Overview of *Wi-Fruit*

Any device with the Wi-Fi transmission module can perform as the transmitter to send Wi-Fi signals. Smart devices with multiple antennas and camera modules perform as receivers that collect Wi-Fi CSIs and fruit images as inputs and process them for final fruit moisture and SSC estimation. According to the received signals penetrating through target fruits deployed on the LoS link between transceivers, *Wi-Fruit* can measure electrical properties from relative amplitude and phase changes among antennas, which are then fused with visual information like fruit size, shape, and type to estimate fruit biological properties. As illustrated in Fig. 6, there

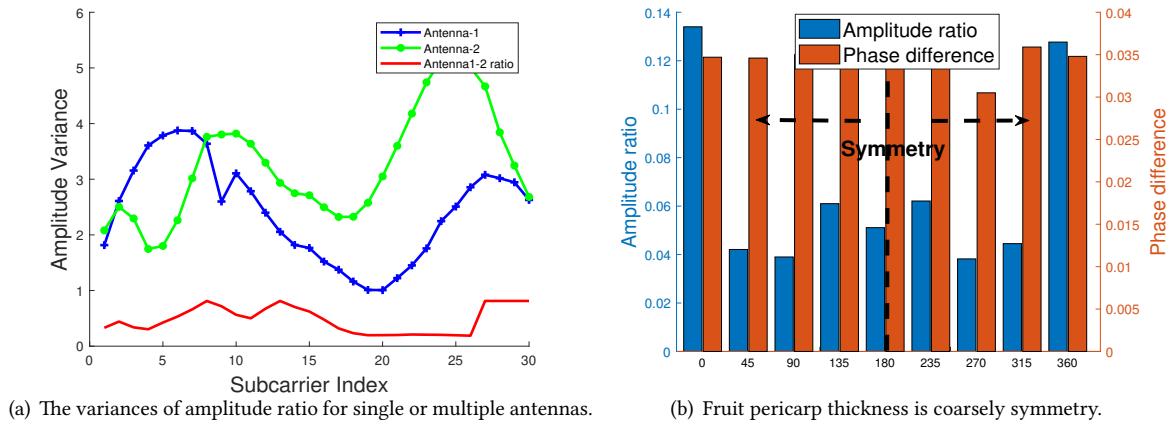


Fig. 7. Observations on neighboring antennas and fruit pericarp thickness.

are two key components in *Wi-Fruit* include (1) a double-quotient model-based CSI pre-processing; and (2) an information fusion-based fruit moisture and SSC estimation.

The **double-quotient model-based CSI pre-processing module** is proposed to process raw CSI readings between neighboring antennas with and without target appearance. This module can denoise the received CSI information and remove the fruit structure dependency (*i.e.*, the first challenge discussed in Section 2.4) as well, ensuring the estimation accuracy for the next module.

The next **information fusion-based estimation module** takes both sensing and visual information as inputs and outputs fruit moisture and SSC measurements via a 3-layer lightweight ANN. The sensing information is acquired from the previous CSI pre-processing module. And the visual information including fruit size, shape, and type is obtained from image processing methods. It assists to remove fruit size and type dependency in estimations, which are the latter two challenges as discussed in Section 2.4. In the following subsections, we will introduce each module in detail.

3.2 Double-quotient Model-based CSI Pre-processing

The raw CSI readings reported by each antenna on the Wi-Fi NICs cannot be directly applied for fruit moisture and SSC measurements due to the bandwidth limitation, signal noise, and fruit structure dependency problems. The absolute amplitude and phase analysis on a single antenna require ultra-wide bandwidth for satisfactory accuracy [21], which is not available in the UHF unlicensed spectrum. Previous work [22, 23, 37, 40, 41] has demonstrated that the high accuracy can be achieved by the relative ToF and AoA analysis among multiple antennas with limited bandwidth, such as Strobe [22], which realized satisfactory measurements on soil moisture and EC with 20MHz-channel and 3-antenna commodity Wi-Fi. Thus, *Wi-Fruit* also utilizes relative amplitude and phase analysis among multiple antennas to overcome bandwidth limitations on commodity Wi-Fi devices.

Our observations based on real-collected CSI have explored several relationships between neighboring antennas on the same receiving chip:

- (1) As observed from Fig. 7 (a), the amplitude ratio between neighboring antennas has the lowest packet variance on all subcarriers compared with amplitude readings for each antenna.
- (2) As observed from Fig. 8 (b), the phase subtracted results between neighboring antennas can aggregate within a small degree range, reducing the randomness shown in the phase of each antenna.

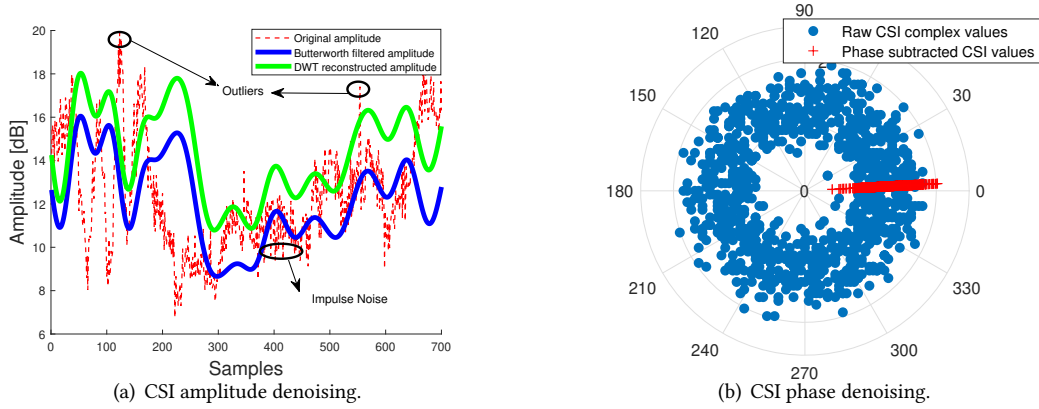


Fig. 8. CSI denoising.

(3) As observed from Fig. 7 (b), the average amplitude ratios and phase subtractions for the watermelon skin (Fig. 4 (b)) are symmetrical evenly, so the measurement on any degree from one side can also represent the one on the symmetrical side. The maximum and the minimum amplitude ratios happen at the minor axis and macro axis of fruits respectively. So in our analysis, we assume that the average values measured at the fruit minor axis and macro axis can represent the measurement on the whole fruit.

According to these observations, the signal noise and fruit structure dependency can be removed between adjacent antennas. It motivates our design of the double-quotient model for CSI pre-processing, which goes beyond the commonly used CSI quotient model [31].

3.2.1 The CSI Quotient Model for Signal Denoising: Background. The CSI quotient model has been widely used for CSI denoising recently [31, 42]. Recall the received waveform representation in Section. 2.3, the quotient model Q for two neighboring receiving antennas is:

$$Q = \frac{A_1 e^{-\alpha} \cdot e^{-j\beta d}}{A_2 e^{-\alpha} \cdot e^{-j\beta(d+\Delta d)}} = \frac{A_1}{A_2} e^{(\phi_1 - \phi_2)}, \quad (8)$$

where A_1, A_2, ϕ_1, ϕ_2 are amplitudes and phases for CSIs collected on antenna 1 and 2 respectively. That is, the quotient value on two receiving waveforms is transformed to the amplitude ratio and phase difference between neighboring antennas. We then show how this quotient model can be used for signal denoising.

For phase denoising, blue dots in Fig. 8 (b) represent raw CSI complex values on one subcarrier of the first receiving antenna collected at one timestamp. It shows the “doughnut” shape implying the randomness of raw CSI phase values, which is caused by asynchronization between transceivers and hardware noises, such as Packet Boundary Delay (PBD) λ_p , Sampling Frequency Offset (SFO) λ_s , Carrier Frequency Offset (CFO) λ_c , and other measurement noises N . Accordingly, we can represent the polluted phase readings $\tilde{\phi}_{k,i}$ for the k th subcarrier on the i th antenna as [23]:

$$\tilde{\phi}_{k,i} = \phi_{k,i} + k(\lambda_p + \lambda_s) + \lambda_c + N. \quad (9)$$

Since different antennas on the same board share the same clock, their PBD, SFO and CFO are identical [43, 44]. We can remove these noises by phase subtraction of neighboring antenna pair and get the relative phase reading $\Delta\tilde{\phi}_k$ on the k th subcarrier: $\Delta\tilde{\phi}_k = \Delta\phi_k + \Delta N$, where ΔN follows Gaussian distribution thus can be removed by

the sliding window average method. As shown by the red cross symbols in Fig. 8 (b), the phase difference values is relatively “clean” without the random noise impact.

For amplitude denoising, as shown in Fig. 8 (a), the raw amplitude readings (represented by the red dot line in this figure) contain substantial outliers, impulse noise, and even missing values in our dataset. They also suffer transmission power inconsistency with respect to time, due to the random power adjustment among Wi-Fi transceivers in changing environments. But no matter how transmission power changed with respect to time, antennas on the same receiving board share the same changing ratio. Therefore, the amplitude ratio for the neighboring antenna pair is transmission power independent. The amplitude denoising ability of the quotient model can be also seen in Fig. 7 (a). The amplitude variances among packages are the smallest for the amplitude ratio when comparing with amplitude values on single antennas. From the above discussions, the CSI quotient model can denoise both amplitude and phase readings.

However, this CSI quotient model cannot be directly used in our scenario due to fruit structure dependency. So we go beyond and propose a double-quotient model introduced in the next subsection.

3.2.2 The Double-quotient Model for Eliminating Fruit Structure Dependency. For better analysis results, we conduct several signal preprocessing steps before the double-quotient model. Considering fruits are measured statically, the noises from outside like potential motions have higher frequencies than the penetrated signals. So the raw CSI readings are first performed by a Fourier Transformation to retain signals with the frequency of 0. Then the amplitude of the left CSI is pre-processed with a Butterworth low-pass filter, which can remove a large number of outliers and impulse noise. We also test the DWT reconstruction used in other material sensing work [23]. It can be seen from Fig. 8 (a) that the Butterworth filter (blue line) performs relatively better as it is less affected by outliers than DWT reconstruction (green line) in our static fruit sensing environment. Such pre-processed CSI signals are further input into the proposed double-quotient model.

Denote the amplitude and phase of the received signals without the target on the LoS link as (A_{air1}, ϕ_{air1}) and (A_{air2}, ϕ_{air2}) for neighboring antenna 1 and 2 respectively. When the fruit is on the LoS link, its amplitude and phase readings are denoted as (A_1, ϕ_1) and (A_2, ϕ_2) for neighboring antenna 1 and 2. As illustrated in Fig. 9, if the thickness of fruit pericarp on the LoS link is d_s , according to the symmetrical feature from the above observation (3), the total length of the pericarp on the LoS link is assumed to be $2d_s$. Especially, for some big-pip fruits such as mango or avocado, the thickness of the pip d_p should also be considered. When the distance between transmitter and receiver is L and the distance between antenna 1 and 2 is ΔL , the amplitude ratio and phase difference for each antenna with and without target are:

$$\frac{A_1}{A_{air1}} = \frac{Ae^{-\alpha_{air}(L-d_1-2d_s-d_p)} \cdot e^{-\alpha_{tar}d_1} \cdot e^{-2\alpha_s d_s} \cdot e^{-\alpha_p d_p}}{Ae^{-\alpha_{air}L}}, \quad (10)$$

$$\frac{A_2}{A_{air2}} = \frac{Ae^{-\alpha_{air}(L+\Delta L-d_2-2d_s-d_p)} \cdot e^{-\alpha_{tar}d_2} \cdot e^{-2\alpha_s d_s} \cdot e^{-\alpha_p d_p}}{Ae^{-\alpha_{air}(L+\Delta L)}},$$

$$\phi_1 - \phi_{air1} = 2\pi \cdot \frac{L - d_1 - 2d_s - d_p}{\lambda_{air}} + 2\pi \cdot \frac{d_1}{\lambda_{tar}} + 2\pi \cdot \frac{2d_s}{\lambda_s} + 2\pi \cdot \frac{d_p}{\lambda_p} - 2\pi \cdot \frac{L}{\lambda_{air}},$$

$$\phi_2 - \phi_{air2} = 2\pi \cdot \frac{L + \Delta L - d_2 - 2d_s}{\lambda_{air}} + 2\pi \cdot \frac{d_2}{\lambda_{tar}} + 2\pi \cdot \frac{2d_s}{\lambda_s} + 2\pi \cdot \frac{d_p}{\lambda_p} - 2\pi \cdot \frac{L + \Delta L}{\lambda_{air}}. \quad (11)$$

Assuming the fruit has a uniform pericarp thickness and pip shape, penetration paths happens in fruit pericarp d_s and pip d_p are the same for adjacent antennas. So we can remove their effects by a further division operation between two antennas:

$$A_q = \frac{A_1}{A_{air1}} \cdot \frac{A_{air2}}{A_2} = e^{-(\alpha_{tar}-\alpha_{air})(d_1-d_2)}, \quad (12)$$

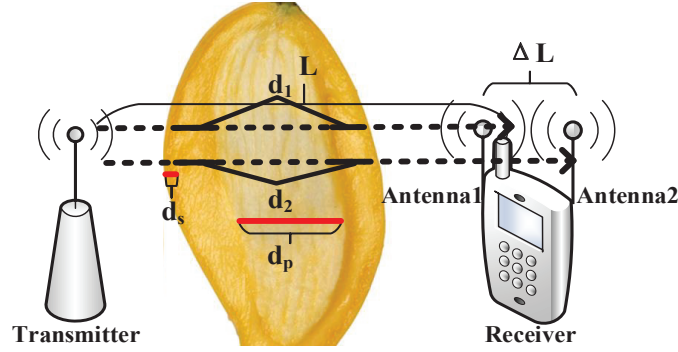


Fig. 9. The CSI sampling illustration.

$$\begin{aligned}
 \phi_q &= (\phi_1 - \phi_{air1}) - (\phi_2 - \phi_{air2}) \\
 &= 2\pi \cdot (d_1 - d_2) \left(\frac{1}{\lambda_{tar}} - \frac{1}{\lambda_{air}} \right) \\
 &= (d_1 - d_2)(\beta_{tar} - \beta_{air}).
 \end{aligned} \tag{13}$$

In a word, the double-quotient model is presented as:

$$Q' = \frac{Q_{1 \leftrightarrow air1}}{Q_{2 \leftrightarrow air2}} = A_q e^{\phi_q}, \tag{14}$$

where $Q_{1 \leftrightarrow air1}$ denotes the quotient model for receiving waveforms on antenna 1 with and without fruit existence, and $Q_{2 \leftrightarrow air2}$ is for antenna 2. According to the discussions in previous section 3.2.1, the amplitude ratio and phase difference values acquired from this double-quotient model have been denoised and at the meantime, the effects of fruit pericarp and pip are also removed from function 12 and 13.

The phase difference ϕ_q and amplitude ratio A_q acquired from the quotient model are then expected to remove the multi-path impact. The 40MHz bandwidth of WiFi channels in our paper results in a distance resolution of 7.5 meters when the wireless signal travels at the speed of light. In typical indoor environments, the acquired first-arrival CSI would suffer from the multi-path impact, which is the mixture of signals penetrated through, scattered from fruits, and reflected from surroundings. To deal with this problem, subcarriers with smaller variance across packets are selected, which are considered to be less affected by multi-path [23]. The final phase difference $\bar{\phi}_q$ and amplitude ratio \bar{A}_q values are averaged from the selected subcarriers for the next biological feature estimation procedure. Subcarriers are selected for each measurement, so they can deal with the changing surroundings. Besides, this subcarrier selection strategy can also help to remove the missing value impact in CSI readings, as subcarriers containing missing values have larger packet variance and would not be selected for the final calculation. According to our real tests, we select 4 subcarriers with minimum variances to get satisfactory measurement accuracy.

3.3 Information Fusion-based Biological Feature Estimation

Illustrated by function 6 and 7, the fruit moisture M and SSC level S can be estimated when knowing the apparent permittivity ϵ_a and the apparent EC θ_a . And according to function 4 and 5, the measurements of ϵ_a and θ_a rely on the phase change factor β_{tar} and the amplitude change factor α_{tar} respectively. If we ignore the fruit size dependency and possible deployment differences, β_{tar} and α_{tar} can be directly calculated by removing the dependency of $(d_1 - d_2)$ in function 12 and 13 with the following equations. Denote the processed amplitude ratio

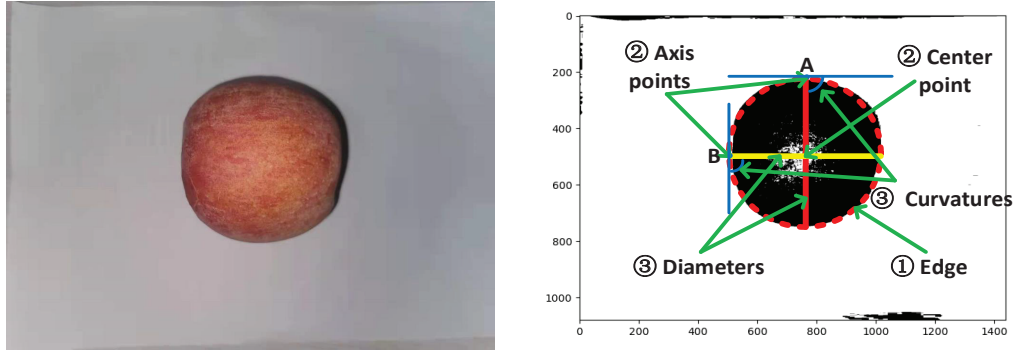


Fig. 10. Image processing based fruit size and shape analysis. [The left figure is the camera captured image and the right figure is its processed binary image with illustrations.]

and phase change acquired at the target timestamp are $\{\bar{A}_{q1}, \bar{\phi}_{q1}\}$ and ones at another timestamp are $\{\bar{A}_{q2}, \bar{\phi}_{q2}\}$, we have:

$$\frac{\ln \bar{A}_{q1}}{\ln \bar{A}_{q2}} = \frac{\ln e^{-(\alpha_{tar} - \alpha_{air})(d_1 - d_2)}}{\ln e^{-(\alpha'_{tar} - \alpha_{air})(d_1 - d_2)}} = \frac{\alpha_{tar} - \alpha_{air}}{\alpha'_{tar} - \alpha_{air}}, \quad (15)$$

$$\frac{\bar{\phi}_{q1}}{\bar{\phi}_{q2}} = \frac{(d_1 - d_2)(\beta_{tar} - \beta_{air})}{(d_1 - d_2)(\beta'_{tar} - \beta_{air})} = \frac{\beta_{tar} - \beta_{air}}{\beta'_{tar} - \beta_{air}}. \quad (16)$$

The $\{\bar{A}_{q2}, \bar{\phi}_{q2}\}$ and $\{\alpha'_{tar}, \beta'_{tar}\}$ in these functions can be recognized as the anchor values of each fruit type, which are obtained by calculating the average of the collected values in dataset. The biological properties M_{tar} and S_{tar} are further estimated with these anchor values according to function 3, 4, 5, 6, and 7. However, as shown in Table. 2, the estimation accuracy of this anchor-based method is quite low (RMSE = 1.890). It illustrates that although we have acquired sensing results \bar{A}_q and $\bar{\phi}_q$ from the last step, we still cannot accurately calculate M and S due to the following two main challenges mentioned in Section 2.4.

First is the *fruit size dependency*. The calculation of $\alpha_{tar}, \beta_{tar}$ depends not only on the averaged phase difference $\bar{\phi}_q$ and amplitude ratio \bar{A}_q , but also on the penetration path difference $(d_1 - d_2)$ as shown in function 12 and 13. It is intuitive to obtain this path difference values for calculation as how Strobe [22] did. It can be realized when the angle of incidence for transmitted signals is known, but requiring the surface of the soil is controlled to be flat and the penetrated thickness in the soil is also pre-known. However, both the angle of incidence and the penetrated thickness in fruits are difficult to be acquired, because the curvature of fruit surface and the fruit size are various on different fruit samples. So it is changeable to directly calculate the path difference in fruit sensing.

Second is the *fruit type dependency*. Assuming we already have electrical feature measurements (*i.e.*, ϵ_a and θ_a), the mapping from these two electrical measurements to biological properties (*i.e.*, M and S) varies from fruit types. In other words, the function 6 and 7 are not generalized and suitable for all types of fruits.

As both these two challenges can not be addressed only from Wi-Fi sensing information, we found it possible to leverage the widely deployed camera module on smart devices to provide fruit size, shape, and type information from the visual dimension. The sizes of fruits are represented by their longest and shortest diameters and the shapes of fruits are represented by the corresponding curvatures. They are acquired from image processing, which are geometric problems in essence. The images of target fruits are captured with a relatively “clean” background where no other objects are in the view to avoid detection interference. A faster median filter is firstly applied to acquire the fruit binary image (as shown in the right figure of Fig. 10). The diameters are calculated from this binary image by the method proposed in [45] with the pre-known camera focal length and

Table 2. Performance of lightweight machine learning models for fruit moisture and SSC estimation.

Index	Model	Parameters	RMSE	R ² score
1	Anchor-based estimation	-	1.890	-
2	Linear Regression	default	0.900	0.218
3	Decision Tree	default	0.939	0.254
4	SVR	default	0.892	0.320
5	KNN Regression	default	0.760	0.393
6	Random Forest	max_depth=5	0.570	0.588
7	XGBoost	max_depth=3, lr=0.1	0.66	0.338
8	LightGBM	num_leave=32, lr=0.1	0.758	0.414
9	GBDT	n_estimators=200,max_depth=11,lr=0.1	0.744	0.452
10	3-layer ANN	{32,16,2},lr=1e-5,iter=1000	0.319	0.856

shooting distance. The edge is detected with the 8-connected boundary tracking method where the center and axis points are located for further diameter and curvature acquisition. Due to the symmetric shape for most fruits, we only extract the longest and shortest diameters of fruits. Then the curvature set can also be calculated once finding the edge sequence points. We finally preserve two curvatures at the point corresponding to the longest and shortest diameters (the point A and B as shown in Fig. 10). To further obtain the fruit type information, we leverage a state-of-the-art 13-layer CNN [46] as the back-end to output fruit types from the captured images.

Until now, the multi-dimension knowledge we have before biological feature estimation is from both sensing and vision dimensions. That is, the amplitude change factor \bar{A}_q , the phase change factor $\bar{\phi}_q$, the shortest and longest diameters denoted as D_s and D_l , the corresponding curvatures C_s and C_l , and the fruit type T . As the ground truth, we collect their corresponding moisture and SSC levels in situ with portable devices (*i.e.*, the penetrometer Jacks JK-100R for moisture measurements and the refractometer Mileseeey SM20 for SSC measurements) in a destructive manner. The biological feature estimation is essentially a regression problem, taking a five dimension inputs $\{\bar{A}_q, \bar{\phi}_q, D, C, T\}$ to predict a two-dimension outputs $\{M, S\}$.

Mathematically, this regression problem can be regarded as a supervised learning problem with input X and its label Y . Each fruit i builds two inputs at each collection timestamp t when the shortest (s) and longest (l) diameters appear on the LoS link, that is, $X^s(i, t) = \{\bar{A}_{tar}^s(i, t), \bar{\phi}_{tar}^s(i, t), D^s(i), C^s(i), T(i)\}$ or $X^l(i, t) = \{\bar{A}_{tar}^l(i, t), \bar{\phi}_{tar}^l(i, t), D^l(i), C^l(i), T(i)\}$. The labels for $Y^s(i, t)$ and $Y^l(i, t)$ are the same combination of $M(i, t)$ and $S(i, t)$ denoted as $Y(i, t) = \{M(i, t), S(i, t)\}$. We apply the one-hot coding for the input $T(i)$ and conduct data normalization for a better regression performance. For COTS device adaptation, a lightweight regression model is required. We have tried 9 lightweight machine learning models and summarize their performance in Table 2. It is obvious that the dataset shows its nonlinearity where the R² score of linear regression model is lowest (0.218). And a 3-layer ANN model outperforms other nonlinear regression models with the highest prediction accuracy (RMSE=0.319) and model relevance (R² score=0.856). It is a powerful tool to dig out potential features in data due to its self-learning, state-association memory, and fast optimization ability. Our lightweight ANN model consists of three dense layer with 32, 16, and 2 outputs, corresponding to 416, 528, and 34 parameters respectively. They are fully connected layers with flat number of hidden units. The activation function for the latter two layers is the Relu function, and the optimizer of our model is Adam in Tensorflow.

4 IMPLEMENTATION DETAILS

In this section, we introduce the prototype of *Wi-Fruit* and discuss some implementation issues. Considering that implementation issues mainly happen in the Wi-Fi sensing stage, we utilize the amplitude ratio and phase difference output from the double-quotient model to show impacts on different setups.

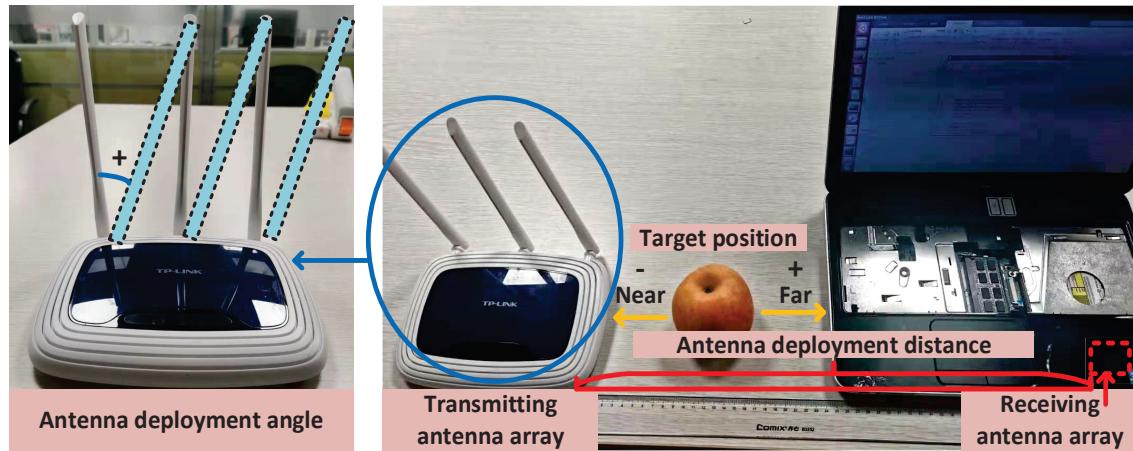


Fig. 11. The prototype of *Wi-Fruit*.

4.1 Prototype Setups

To conduct extensive evaluations on *Wi-Fruit*, we implement a prototype shown in Fig. 11. A commodity 3-antenna Wi-Fi router is the transmitter and a laptop with an embedded 2-antenna Intel 5300 wireless card is the receiver. Besides, a mobile phone with a 12 megapixel (MP) master camera and a 5 MP slave camera is used to capture target fruit images. The router works in 802.11n AP mode at 5.24GHz frequency with 40MHz bandwidth. The laptop operates with 64bit Ubuntu 14.04 LTS system, 2.5GHz CPU, and 3.7GB memory.

When the target fruit is deployed on the LoS link of transceivers, the raw CSI is collected by the Linux CSI Tool [38] on the laptop. The target images captured by the mobile phone are sent to the laptop for image processing through Wi-Fi connections. The double-quotient model-based CSI pre-processing is coded on Matlab 2016a. The information fusion-based estimation includes the image processing and ANN estimation is coded with Python on Pycharm Community Edition 2020. All these data processing codes are running on the receiver side (*i.e.*, the laptop in this prototype) for acquiring the final fruit moisture and SSC values.

4.2 Implementation Issues

In this subsection, we will discuss several implementation issues with the prototype shown in Fig. 11. Proper setups are selected from these discussions for better fruit moisture and SSC estimation performance in real deployments.

4.2.1 Antenna Deployment Distances. As shown in Fig. 11, the straight-line distance between the transmitting antenna array and the embedded receiving antenna array is one of the design issues. Considering the general sizes of the COTS fruit scales, which range from 35cm to 60cm, we evaluate CSI differences by changing the distance from 35cm to 70cm while putting a watermelon with an 18cm diameter on the LoS link. It can be seen from Fig. 12 (a) that the amplitude ratio and the phase difference do not change sharply after the distance of 55cm. It can be explained that under the 5.7cm wavelength for 5.24GHz Wi-Fi communication, the watermelon with an 18cm diameter can be entirely covered in the first Fresnel Zone [42] when the distance between transceivers is 56.84cm. To adapt to most of the fruit scales in the market, we choose **60cm** as the antenna deployment distance.

4.2.2 Antenna Deployment Angles. The antenna deployment angle describes the angle between the antenna array and the table. As shown in the left figure of Fig. 11, we consider the angle is 0 when the antenna array is perpendicular to the table, and the angle is positive when the antenna array rotates to the right side and

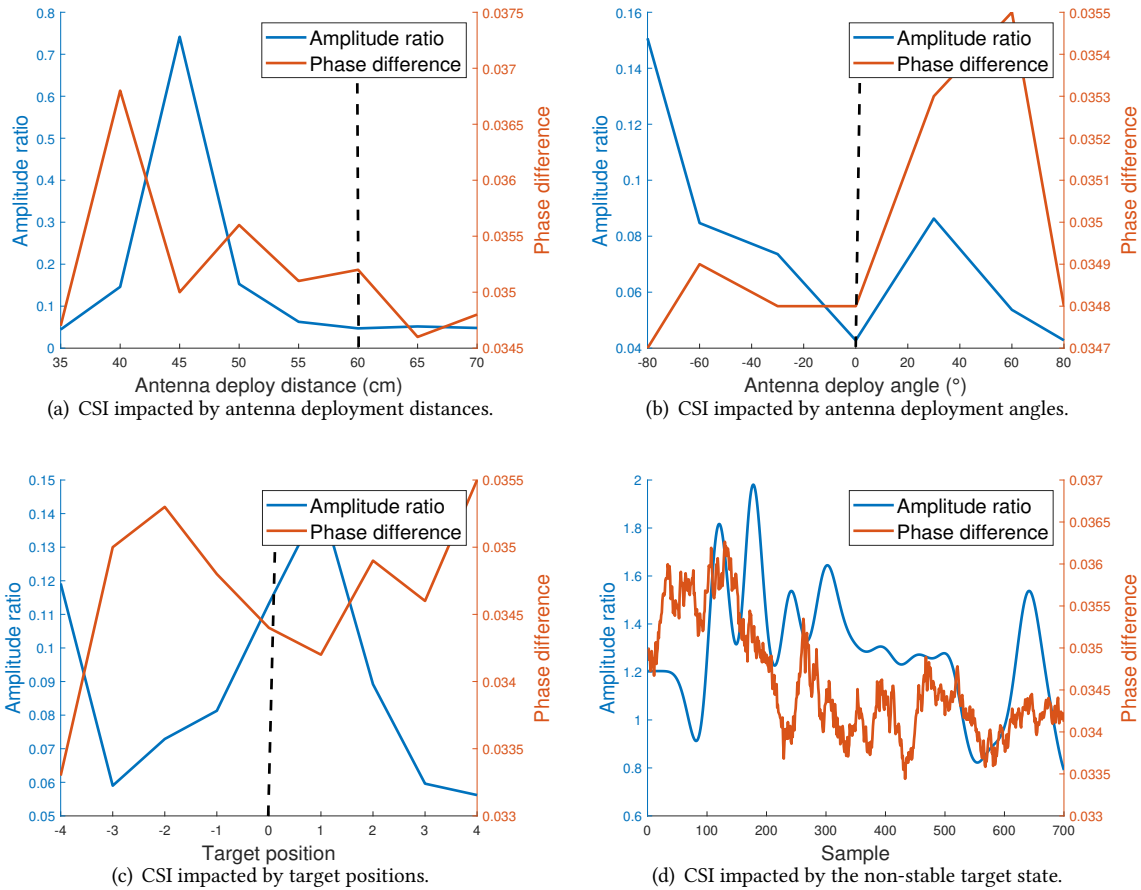


Fig. 12. The CSI performance on implementation issues.

vice versa, where the absolute value represents the rotation angle. Results shown in Fig. 12 (b) illustrate that different deployment angles will greatly impact CSI information. In this paper, the deploy angle is kept to be **0 (perpendicular)** for the following measurements.

4.2.3 Target Positions. When the axis of fruits falls at the center point between transceivers (*i.e.*, 30cm away from the transmitter), the target position is denoted as “0” in the paper. The position is positive when the fruit is far away from the transmitter and vice versa, where the absolute value represents the multiple of the moving distance (*i.e.*, 5cm). The impacts on CSI with respect to different positions of targets are presented in Fig. 12 (c). It is obvious that slight changes in target positions will cause non-monotonous changes in amplitudes and phases, but when $-3 < x < 1$, the amplitude ratio keeps increasing possibly due to more signals bypassing the target surface are received. To ensure the target material can impact more on the receiving signals, the object should be placed closer to the transmitter [37]. So the axis of fruits is decided to fall at the point which is **15cm** away from the transmitter (*i.e.*, “ $x = -3$ ” in Fig. 12 (c)) in real deployments.

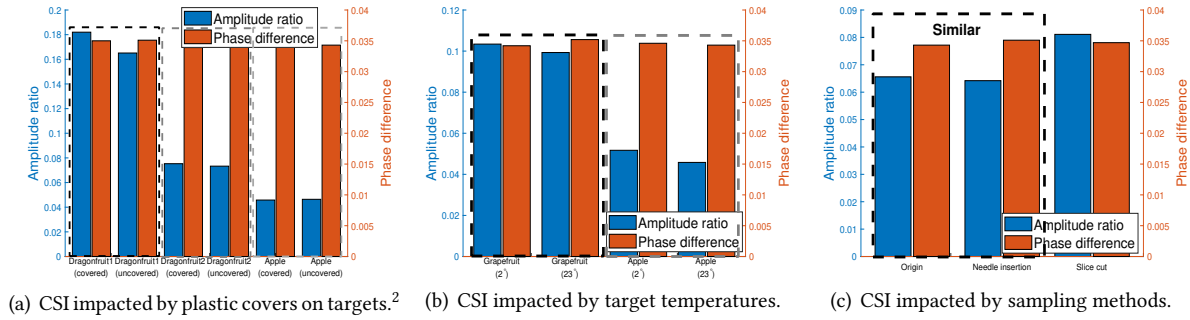


Fig. 13. The impacts of CSI on practical design choices for targets.

4.2.4 Target States. It is unavoidable in a practical sensing scenario that the CSI is collected while the target fruit is not in a stable state. Fig. 12 (d) shows that both amplitude ratio and phase difference fluctuate following the movement of the target. So the CSI is required to be collected after the target is **kept stable** in our paper.

4.2.5 Plastic Covers on Targets. In order to prolong the freshness of fruits, fruit retailers often put a layer of plastic wrap on some damaged fruits, such as a cut watermelon. Evaluation results in Fig. 13 (a) proves that such thin plastic wrap causes a negligible impact on processed CSI results with our method. It can be seen that the amplitude ratio and phase difference values for the same fruit with and without cover are **quite similar**. Thus, we also adopt this preservation method on our fruit samples for CSI collection in a longer period.

4.2.6 Temperatures of Targets. Similar to plastic covers, it is also common to put fruits in refrigerators for extending their preservation time. Evaluations on two kinds of fruits (*i.e.*, grapefruit who has thicker pericarp and apple who has thinner pericarp) have been summarized in Fig. 13 (b). The measurements of CSI with only temperature difference (*i.e.*, 2°C and 23°C) for each kind are slightly different. The impacts on fruits with thick pericarps like grapefruits are larger than ones with thin pericarps like apples. It can be understood that fruit pericarps and pulps have different chemical components, and the thicker pericarps will result in a larger impact on CSI analysis for pulps. For a better evaluation performance, the CSI will be collected when the temperatures of fruit samples are consistent with the **room temperature** after taking out from the refrigerator.

4.2.7 Sampling Methods on Targets. As the collection of ground truth moisture and SSC levels is performed on fruit samples, which cause damage to the fruit structure, we need to decide on a sampling method to cause the minimum damage and impact on CSI compared with its original form. We have considered two sampling methods: 1) Cut a small piece of fruit and put it back after measurement to ensure structural integrity; 2) Insert a **needle syringe** to extract a pulp sample. Evaluation results shown in Fig. 13 (c) prove that the second method can cause less impact on the sensitive CSI, which becomes our choice for ground truth collection.

²Note that “Dragonfruit1” and “Dragonfruit2” are collected when the longest and shortest diameters appear on the LoS link for the same fruit respectively.

5 PERFORMANCE EVALUATION

We conduct extensive evaluations to validate the efficiency of *Wi-Fruit* on non-destructive and low-cost fruit moisture and SSC estimation. In this section, we will introduce evaluation setups and report results with analysis. At the end of this section, we present two case studies corresponding to potential application scenarios introduced in Section 2.1 to further illustrate the real-world deployment of *Wi-Fruit*.

5.1 Evaluation Setups

5.1.1 Hardware setups. Evaluations are conducted on the prototype shown in Fig. 11. According to the discussions of implementation issues, in our evaluations, the transceivers are placed with a distance of 60 cm and the transmitting antennas are perpendicular to the tabletop.

5.1.2 ANN Parameters. The ANN model is a fully connected network with 3 dense layers. The learning rate is $1e^{-5}$ and the epoch is 1000. 20% dataset is split as the testing set and others build the training set.

5.1.3 Fruit Samples and Treatments. We select 6 kinds of fruits categorized into thick skin and thin skin groups. The fruits in the thick skin group are watermelons and grapefruits, while the ones in the thin skin group are apples, pears, oranges, and dragon fruits. We have collected CSI and ground truths of 20 items for each kind during a one-month period in total with 12 hours gap. These fruits are stored under 2°C in the refrigerator for preservation. Each item stored in the fridge is separated and sealed by PE fresh-keeping films which are changed after every measurement. It aims to reduce any possible cross-infection (*e.g.*, ethylene volatilization effect) and microbial infection, and prolong the lifespan of fruits. All fruits will be placed under the room temperature (*i.e.*, 23°C) for half an hour before measurements. They will also be washed with tap water to remove any dust or soil material and wiped to dry for next measurements.

5.1.4 Ground Truth Collection. Two ground truth values are measured for evaluation: fruit moisture and SSC. They are collected with COTS devices on fruit internal tissues extracted with the syringe. The moisture is measured by a penetrometer SmartSensor AR991 with 0.1% accuracy, and the SSC is measured by a refractometer Mileseeey SM 20 with 0.2% accuracy. The mirror of the refractometer and the probe of the penetrometer are calibrated with de-ionized water and dried in the air before any measurement.

5.1.5 Dataset Collection. The CSI measurements are received every 10 seconds with the 100pkt/s package rate. The datasets are collected in two environments: an empty laboratory and a library with massive books, representing low and high multi-path impacts respectively. The CSI and its ground truth pairs are collected every 12 hours within a week as we found that our fruit samples with slight damage will rot in about a week. The CSI without fruit deployment (*i.e.*, signal penetrates only in the air) will be collected before every measurement at each collection timestamp. And CSI readings for target presence are then collected when it keeps stable.

5.2 Evaluation Results

We conducted extensive evaluations on *Wi-Fruit* in the following aspects:

- (1) **Estimation Accuracy:** The estimation accuracy is measured with the Root Mean Square Error (RMSE) with respect to moisture and SSC ground truth values.
- (2) **Fruit type independence:** This independence is measured from the accuracy for different types of fruits with various moisture and SSC levels.
- (3) **Fruit structure and size independence:** This independence is measured from the estimation accuracy for fruits with different thicknesses of pericarps and different sizes.
- (4) **Time robustness:** The time robustness is measured with the estimation accuracy on data collected on different days.

Table 3. Performance on overall estimation accuracy with multiple contrast evaluations.

Method	Difference with <i>Wi-Fruit</i>	RMSE	R ² score
ANN + information fusion	Ours	0.319	0.856
ANN + sensing information	The amplitude and phase values are inputs.	0.422	0.039
ANN + visual information	The diameters, curvatures, and types are inputs.	0.341	0.322
ANN + moisture	The moisture is the output.	0.745	0.445
ANN + SSC	The SSC is the output.	0.516	0.733

- (5) **Environment robustness:** The environment robustness is measured with the estimation accuracy on data collected in two environments with different multi-path impacts.

5.2.1 Contrast Evaluations on Overall Biological Feature Estimation Accuracy. We discuss the estimation accuracy of *Wi-Fruit* by comparing it with the following methods, and their performance is summarized in Table 3:

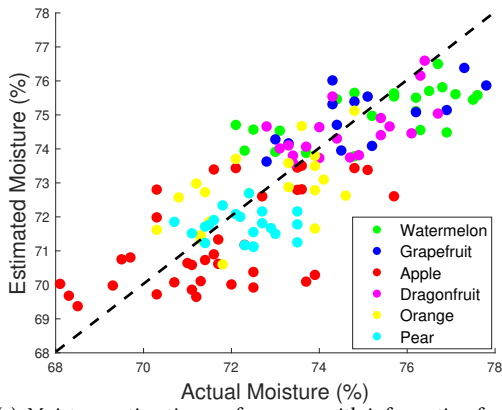
- (1) ANN on sensing information: We only take $\{\bar{A}_{tar}(i, t), \bar{\phi}_{tar}(i, t)\}$ as inputs to train our proposed ANN model, which are acquired from the double-quotient model-based CSI pre-processing module.
- (2) ANN on visual information: We only take $\{D(i), C(i), T(i)\}$ provided by the image processing module to train our proposed ANN model for estimation.
- (3) ANN training only with moisture: We only take $Y = M$ to train the proposed ANN.
- (4) ANN training only with SSC: We only take $Y = SSC$ to train the proposed ANN.

Results in Table 3 have shown the superiority of the accuracy of our proposed ANN with information fusion. On the one hand, training on sensing and visual information fusion provides higher accuracy than training on individual dimensions as shown in rows 1, 2, and 3. We further present the estimation performance of these three methods in Fig. 14, where Fig. 14 (a, b) are for information fusion estimation, Fig. 14 (c, d) are for sensing information-based estimation, and Fig. 14 (e, f) are for visual information-based estimation. Compared with the information fusion estimation, the sensing-based estimation dots for various kinds of fruits fall within a small area (*i.e.*, (71, 76) for moisture, (8, 12) for SSC). Because to cope with the bandwidth limitation of Wi-Fi, we analyze relative amplitude and phase values among multiple antennas, which ignore the fruit type and size impacts. On the contrary, the vision-based estimation can distinguish among different fruit kinds, but it has a relatively low estimation accuracy than fused estimation since it ignores fruit structure dependency.

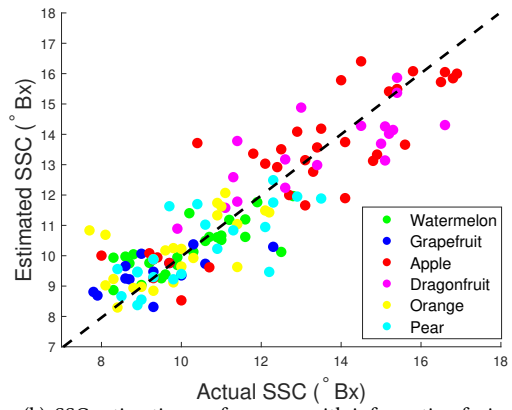
On the other hand, training with moisture and SSC aggregation achieves higher accuracy than training with the single label as shown in the 4th and 5th row. It is consistent with the observations reported in researches [47–49] that fruit moisture and SSC levels are correlated with each other. So the model built on these two factors utilizes their correlations to increase estimation accuracy mutually.

5.2.2 Fruit Type Independence. The overall moisture and SSC estimation results for our collected 6 fruit types are presented in Fig. 14 (a) and (b) respectively. It can be seen that the estimation accuracy of all fruit types are satisfactory as they are approaching the $y = x$ line, illustrating the fruit type independence. Specifically, we further validate the overall estimation accuracy with RMSE for each fruit type and summarized in Table. 4. *Wi-Fruit* realizes fruit type independence because it obtains the fruit type information from the image processing module and takes it as one of the inputs of the ANN estimation model. Thus, the estimated results are related to features corresponding to each specific fruit type. The fruit type independence of *Wi-Fruit* makes it extendable to other fruits as long as their ground truth values are collected for model training.

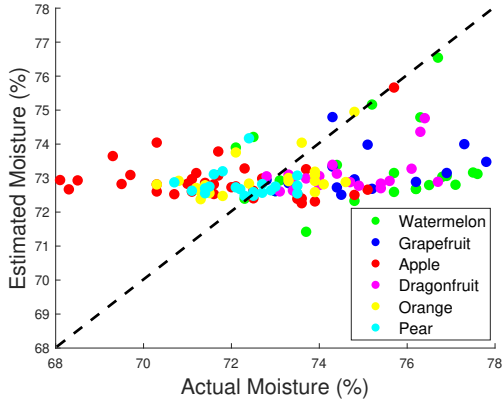
5.2.3 Fruit Structure and Size Independence. To evaluate the fruit structure and size independence, we first select two types of fruits in our dataset: watermelons and apples, which represent thick and thin pericarps respectively. Their biological properties are estimated when (i) keeping their completeness, (ii) removing their pericarps, (iii)



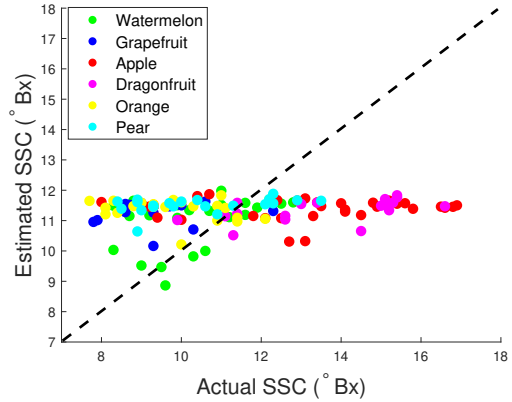
(a) Moisture estimation performance with information fusion.



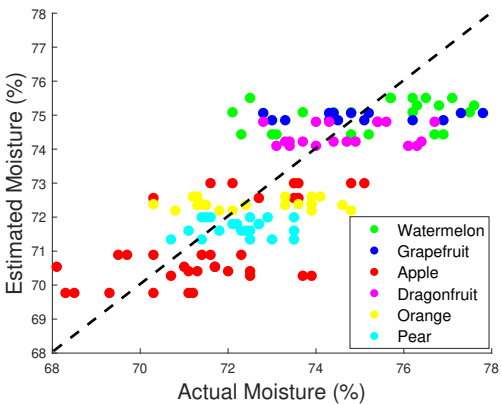
(b) SSC estimation performance with information fusion.



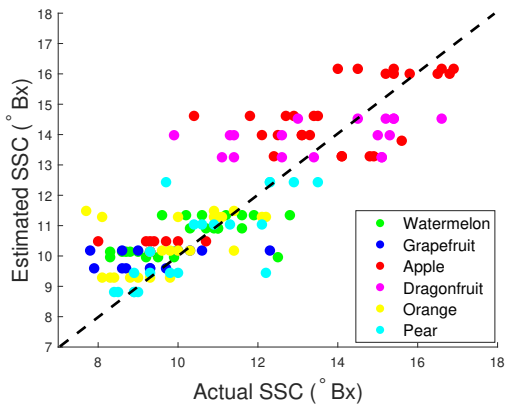
(c) Moisture estimation performance with only sensing information.



(d) SSC estimation performance with only sensing information.



(e) Moisture estimation performance with only visual information.

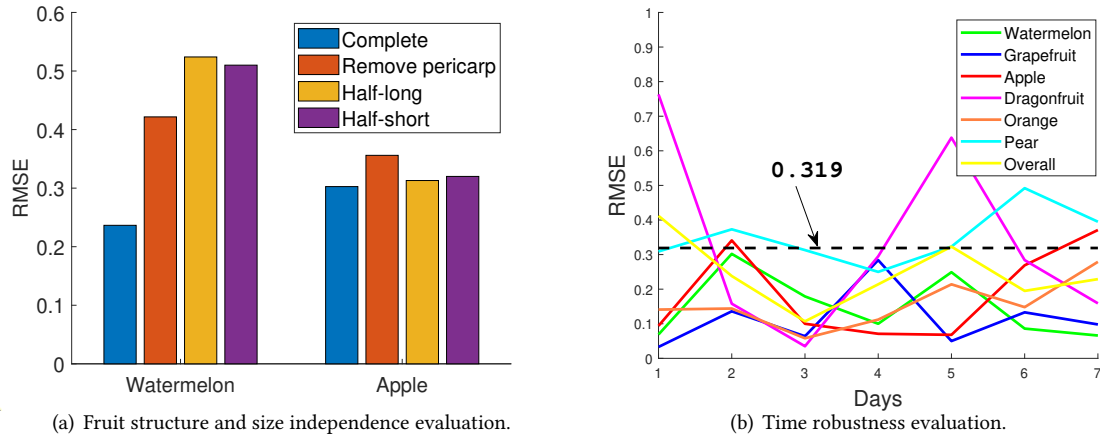


(f) SSC estimation performance with only visual information.

Fig. 14. Biological feature estimation performance for various fruit types with different inputs.

Table 4. Performance on fruit type and structure independence and environment robustness.

Fruit type & structure independence						
Type	Watermelon	Grapefruit	Apple	Dragon fruit	Orange	Pear
RMSE	0.293	0.447	0.574	0.473	0.515	0.661
Euclidean Distance	0.854	0.913	0.171	0.169	0.257	0.164
Environment robustness						
Environment	Empty Laboratory			Library with massive books		
RMSE	0.319			0.520		

Fig. 15. Evaluations of *Wi-Fruit* on fruit structure and size independence as well as time robustness.

cutting them to half and deploying its longest axis on the LoS, and (iv) deploying the shortest axis of the half fruit on the LoS. The estimation accuracy under four conditions is presented by RMSE results in Fig. 15 (a), where the RMSE values are similar for all manual processing. Specifically, the fruit structure independence is implied from blue and red bars in this figure, where the estimation accuracy is similar with or without pericarps. And the fruit size independence is implied by blue, yellow, and purple bars, where the estimation accuracy after cutting fruits to half has a slight difference with measurements on complete targets.

Additionally, we examine the performance of *Wi-Fruit* when measuring targets from different angles. After deploying the longest or the shortest axis on the LoS, the similarity of two estimation results is calculated by the average Euclidean distance. The quite short Euclidean distances presented in Table. 4 illustrate that *Wi-Fruit* can achieve fruit structure independence, where the estimated values are robust regardless of the detection angle of targets on the LoS.

5.2.4 Time Robustness. To evaluate the robustness of our method on time, we divide our test dataset into 7 sets containing data collected from 7 continuous days (a week). The estimation accuracy for each fruit kind in 7 days is presented by RMSE values in Fig. 15 (b). It can be seen that the estimation accuracy for most fruit types keeps high during a week which is around the overall estimation accuracy (RMSE = 0.319). So our method can be applied at any time and gives accurate results in situ.

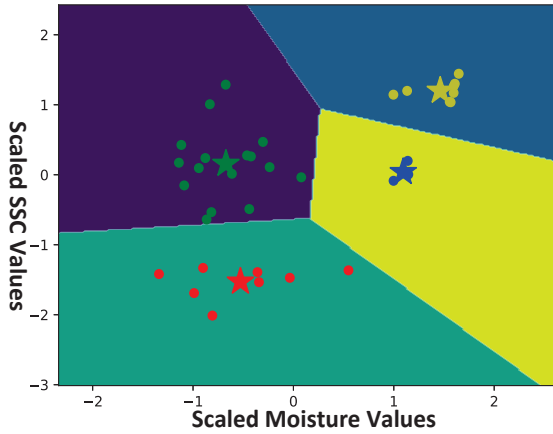


Fig. 16. Clustering results for apples in case study I.

Table 5. The fruit internal quality classification accuracy of estimated moisture and SSC values.

Level	Precision	Recall	F1-score
0	0.94	0.60	0.73
1	0.97	0.89	0.93
2	0.78	0.91	0.84
3	0.57	0.86	0.69
Overall accuracy	0.80		
Macro avg	0.82	0.81	0.80
Weighted avg	0.84	0.80	0.81

5.2.5 Environment Robustness. As we have collected data from two environments: an empty laboratory and library with massive books, we divide the test dataset into two sets and estimate with our proposed ANN model. As summarized in Table. 4, the RMSE for data collected in an empty laboratory is 0.319 and the one for data collected in the library is 0.520. Because the multipath impact is dealt with in *Wi-Fruit*, the estimation errors are similar in these two environments, illustrating the environment robustness of the system.

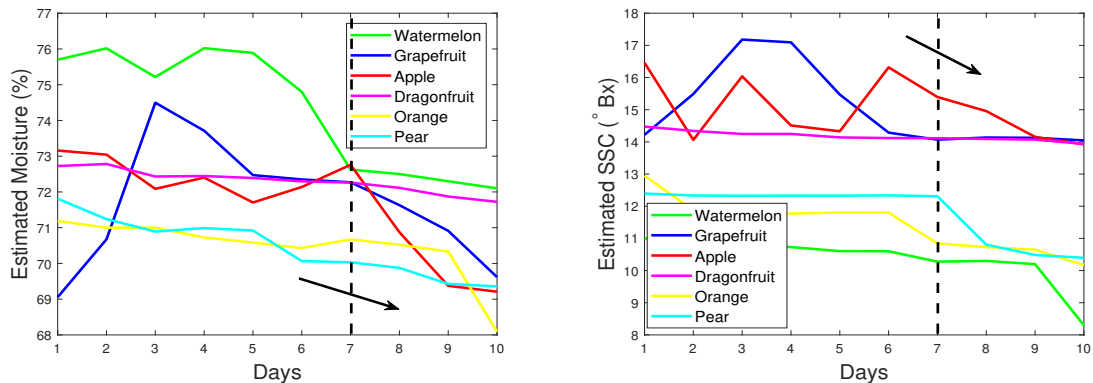
5.2.6 System Overhead. The system overhead is evaluated from the latency and cost aspects. The **latency** is required to be low for *Wi-Fruit*, as a relatively short feedback time after data collection is preferred for daily use. The overall system latency of *Wi-Fruit* after CSI and image collection is the sum of the latency for two proposed modules: double-quotient model-based CSI pre-processing and information fusion-based estimation. In our evaluations, the average latency for double-quotient model-based CSI pre-processing is 2.03s and the one for information fusion-based estimation is 2.17s. So the overall latency is determined as 4.2s without the consideration of data transmission latency between modules as it can be further removed by system integration.

Additionally, the **cost** of the overall system is mostly spent on physical setups including a Wi-Fi transmitter such as a commodity router (cost around 40 US dollars) and a smart device with Wi-Fi and camera modules such as smartphones or tablets (cost around 310 US dollars). All these devices have been widely deployed in our daily life and no other specialized devices are required, so we consider the cost of *Wi-Fruit* is extremely low.

5.3 Case Study I: Fruit Internal Quality Classification

As mentioned in Section 2.1, the first potential application of *Wi-Fruit* is for consumers to pick fruits with high qualities. The manual selection depends mainly upon the external features of fruits, but it is common to pick good-looking but tasteless items. *Wi-Fruits* provides a low-cost solution to classify fruits with their internal qualities, measured by fruit moisture and SSC levels.

To validate its feasibility, we firstly label our experimented fruit samples with K-means clustering algorithm [50], taking the ground truth values of the fruit type, moisture, and SSC as inputs. In this validation, we attempt to classify fruit qualities into 4 levels. One of the labeling examples is shown in Fig. 16. It can be observed that 4 centers of clustering in this figure are corresponding to 4 levels for apples: low moisture and SSC, low moisture but high SSC, high moisture but low SSC, high moisture and SSC. Then we take the same inputs and these labels to train a KNN classifier [51] for fruit internal quality classification. The estimated fruit moisture and SSC values from *Wi-Fruit* together with the fruit type are input into this trained KNN classifier. The classification results



(a) Non-destructively estimated moisture values for different kinds of fruits in case study II. (b) Non-destructively estimated SSC values for different kinds of fruits in case study II.

Fig. 17. Case study II results.

will then be compared with the labeling data of the ground truth values as summarized in Table 5. These results illustrate that the estimated moisture and SSC values from *Wi-Fruit* can achieve 80% accuracy on fruit internal quality classification. Thus, *Wi-Fruit* can provide fruit internal quality information for consumers when picking fruits, making it no longer a lottery-like behavior. It can also help fruit retailers carry out tiered pricing to meet the needs of different types of customers in order to maximize profits.

5.4 Case Study II: Fruit Internal Quality Prediction and Storage Suggestion

The non-destructive measurement of *Wi-Fruit* makes it possible to monitor the changing trend of fruit moisture and SSC values when actual fruits gradually deteriorate at room temperature. In this case study, we every day estimate fruit moisture and SSC values on six fruit kinds (*i.e.*, watermelon, grapefruit, apple, dragon fruit, orange, pear), ten samples each in a month with *Wi-Fruit*. All fruit samples are stored at room temperature (*i.e.*, 23°C). Denote the day when fruits show obvious wrinkles or spoilage spots on pericarps as an anchor. Dragon fruits are observed to have the shortest time from the purchase day to the anchor day, which is only 7 days on average. Thus, we present the average values of estimated moisture and SSC in seven days including the anchor day and three days after in Fig. 17. These figures have revealed the following phenomena:

- (1) Both moisture and SSC values decrease when fruit pericarps are approaching decay. (We also label it with black arrows in two figures.)
- (2) The moisture and SSC values for some fruit kinds (*e.g.*, watermelons and grapefruits in these figures) are not monotonically decreasing. Sometimes it shows a trend of rising first and then falling because these fruits are still in the process of maturity after purchase.
- (3) Although pericarps of some fruits like dragon fruits show obvious signs of decay on the 7th day in these figures, their moisture and SSC values slightly drop after this day. Through cutting, it is found that the inside of the fruit has not rotten at this time.

According to these observations, different kinds of fruits have different recommended storage periods. The fruits with continuously descending moisture and SSC values are recommended to be consumed as soon as possible. For some fruits with thick pericarps, the recommended storage time based on internal feature estimation is slightly longer than the recommendation only based on appearances. Therefore, *Wi-Fruit* can be applied in fruit internal quality prediction and provide storage suggestions for regular customers or small retailers.

6 RELATED WORK

Recent advances have been made on non-destructive fruit quality assessment, from both external and internal evaluations [7, 34]. External factors include fruit type, size, shape, weight, firmness, smell, surface color, and features (e.g., mildew spots). The Doppler laser vibrometer (LDV) [52] is designed to accurately measuring surface texture changes of fruits with the reflected laser beam at a very early age. Nowadays, vision-based technologies [5–8] are widely adopted to provide comprehensive external evaluations with the help of image processing and deep learning, while their performance is sensitive to environmental illumination conditions.

It is inaccurate to assess fruit quality only by external factors. Fruit internal factors describe its chemical components and features, including moisture, SSC, water activity, the content of fat, fiber, etc. Spectroscopy [14, 53] is a classical method for analyzing the internal fruit patterns from electromagnetic radiation with a chemical substance. It emits NIR signals to the surface of the target fruit and analyzes its internal features from the different absorption, reflection, and scatter degrees. It has been widely applied as spectrometers for non-destructive fruit internal measurements in the market, while it requires high cost and controlled setups for most versions. The ultrasound-based sensing is another attempt at non-destructive fruit internal measurements. Researchers in [54, 55] measure the color and hardness of fruits from this mechanical wave with a programmable bipolar remote ultrasonic pulse generator, while they only achieved around 82% evaluation accuracy on these two features.

By contrast, RF-based methods can realize the non-destructive fruit internal sensing with an easier deployment, lower cost, and relatively high accuracy. The potential RF-based methods have been explored in the material sensing area via various spectrums. TagScan [26], Tagtag [25], and RE-EATS [24] move a big step in this direction with the utilization of RFID devices. LiquidID [27] senses liquid categories with UWB radios. Compared with them, RF-based sensing with commodity Wi-Fi has the lowest cost and easiest deployment, as the Wi-Fi module is widely deployed on smart devices and environments. According to the Cisco Annual Internet Report White Paper updated in 2020 [56], there will be nearly 628 million public Wi-Fi hotspots by 2023, up from 169 million hotspots in 2018 globally. So the sensing with Wi-Fi devices has a wider application range. The ability of Wi-Fi-based material sensing has been explored in baggage detection [37], liquid level sensing and classification [23, 30], as well as soil monitoring [22]. Nevertheless, fruit-oriented substantial challenges including fruit structure, size, and type dependencies cannot be directly solved with these proposed methods.

Toward the most related work in non-destructive RF-based fruit sensing, Ren et al. [20] proposed a machine learning (ML) driven fruit moisture content classification system with 0.75-1.1 terahertz (THz) waves. The transmission of these super-high frequency signals requires a specialized platform like Swissto12 MCK used in their paper, which is not feasible for daily use. Tan et al. [21] built fruit ripeness profiles over 600MHz bandwidth of commodity Wi-Fi at 5GHz, with a lower-cost and satisfactory classification accuracy. But their outputs stay at a coarse ripeness classification level. To the best of our knowledge, the *Wi-Fruit* proposed in this paper is the first Wi-Fi-based fine-grained fruit internal assessment, which measures fruit moisture and SSC levels in a non-destructive and low-cost manner.

7 DISCUSSIONS

In this section, we discuss some limitations in the presented work and give possible extensions for *Wi-Fruit* as the future work. At the end of this section, we provide some other potential applications of *Wi-Fruit* except the ones introduced in case studies.

The first limitation is **the size of the evaluation dataset**, including the limited number of data samples and fruit types. As there are no publicly available CSI datasets measured on fruits, the data samples used for ANN training and testing in this paper are manually collected for 20 items each on 6 types of fruit during a one-month period with 12 hours gap. However, in this collected dataset, items in the same type do not belong to the same sub-type. For example, apples in this dataset are composed of both Red-Fuji and Aksu apple (two sub-types of

Table 6. Discussions on impacts in dynamic environments.

Circumstances	RMSE on electrical properties	RMSE on biological estimations
Static environment	Baseline	
Motions on the LoS	0.134	1.000
Motions away from the LoS	0.088	1.433

apples). The estimation accuracy is lower when we further classify them into sub-types due to fewer samples. But considering that this limitation is a matter of time and human efforts, we believe that more data would be acquired with the spatial and temporal extension usage of *Wi-Fruit*. Through the fine-tuning of our pre-trained ANN model, *Wi-Fruit* can achieve higher estimation accuracy and stronger compatibility on more fruit types. As the future work, an incentive mechanism can be designed to expand the usage scope of *Wi-Fruit* and inspire users to contribute more source data with unknown fruit types. The transfer learning can also help to transfer our pre-trained model to unknown fruit types with limited data acquired from users according to the feature similarity among various fruit types.

The second limitation is sensing in **dynamic environments** with motion impacts. In this paper, we have conducted three methods to reduce motion impacts, including multi-antenna deployment, FFT-based amplitude denoising, and variance-based multipath removal. To validate the performance of dealing with motion impacts, we experiment on several apples and collect their CSI under three circumstances: (i) in a static environment; (ii) performing motions on the LoS between transceivers; (iii) performing motions away from the LoS around transceivers. Taking the data collected and estimated in a static environment as the baseline, the differences of data collected and estimated in dynamic environments (*i.e.*, the latter two circumstances) are measured by RMSE values and summarized in Table 6. The table illustrates that motions indeed have impacts on fruit moisture and SSC estimations but are small. Methods proposed in [40, 57] can help to further eliminate these impacts, which is one of the future directions to improve our work.

The third limitation is **the demanding acquisition of visual information**. The result in Fig. 14 shows that visual information contributes more than wireless information does to estimating biological features of fruits. However, the estimation accuracy using visual information highly depends on the quality of the input fruit images. Our experiment uses our own small-scale private dataset as a proof of concept, while in the real world, capturing high-quality images of target fruits is demanding. As such, investigating how *Wi-Fruit* can perform efficiently with high estimation accuracy without high-quality images is one of the interesting future work directions.

The deployment of *Wi-Fruit* is quite simple and convenient, which only needs to be configured once at the beginning. It can be easily deployed in a variety of practical scenarios. For example, this system can be deployed on a computerized scale in a fruit store, with only an extra camera and a Wi-Fi router. The fruit's picture and CSI information can be collected and processed at the same time during the fruit weighing process, and its internal quality analysis results can be quickly obtained locally.

Thanks to its convenient deployment, *Wi-Fruit* has a wealth of applications. Several post-harvest applications have been discussed before, including fruit internal quality classification, prediction, and storage suggestion. Moreover, fruit moisture and SSC estimations given by *Wi-Fruit* are also beneficial to pre-harvest applications, such as fruit harvest time prediction or fruit planting suggestion. kvikliene et al. [58] found strong relationships between the harvest time and SSC values during ripening. *Wi-Fruit* can provide estimated SSC values after harvest non-destructively, where the exact harvest time can be predicted according to their work. The farmers can also adjust their planting and harvest plan according to the post-harvest moisture and SSC levels. Therefore, we believe that the non-destructive fruit moisture and SSC estimation capabilities provided by *Wi-Fruit* can be of great help in fruit saving and safety career during both pre-harvest and post-harvest stages.

8 CONCLUSION

With the increasing demand for the quality of fruits, the accurate evaluation of fruit quality becomes a hot topic in food saving and safety areas. The external fruit quality evaluation is commonly used for fruit picking in daily life while this evaluation is bias as it ignores the fruit internal quality. As two key features on fruit internal quality assessment, existing solutions on fruit moisture and SSC measurements are either destructive or expensive. In this paper, we design *Wi-Fruit*, a non-destructive and low-cost fruit moisture and SSC measurement system with acceptable accuracy and lightweight deployment. Smart devices with Wi-Fi and camera modules can deploy *Wi-Fruit* in a Wi-Fi transmission environment. It provides accurate estimation results through double-quotient model-based CSI pre-processing and information fusion-based estimation via lightweight ANN. Extensive evaluations and discussions based on data collected in real fruits prove the efficiency of *Wi-Fruit* on high estimation accuracy, fruit type, structure, and size independence, together with time and environment robustness. The estimated moisture and SSC values provided by *Wi-Fruit* can be further used in pre-harvest applications like fruit harvest time prediction or planting suggestion, and post-harvest applications like fruit internal quality classification, prediction, and storage suggestion.

ACKNOWLEDGMENTS

This work was supported in part by NSFC grant 61972253, U1908212, 72061127001, 62172276, 62172276, 61972254, 62172345, the Program for Professor of Special Appointment (Eastern Scholar) at Shanghai Institutions of Higher Learning, and Facebook Research Award. Linghe Kong is the corresponding author.

REFERENCES

- [1] 2021 is the international year of fruits and vegetables, food and agriculture organization (fao), <http://www.fao.org/food-loss-reduction/news/detail/en/c/1362525/> (2021).
- [2] CUBII, Global food waste statistics 2020, <https://cubii.co/en/global-food-waste-statistics-2020/> (Aug. 2020).
- [3] U. E. Programme, Worldwide food waste, <https://www.unep.org/thinkeatsave/get-informed/worldwide-food-waste>.
- [4] B. M. Nicolai, K. Beullens, E. Bobelyn, A. Peirs, W. Saeys, K. I. Theron, J. Lammertyn, Nondestructive measurement of fruit and vegetable quality by means of nir spectroscopy: A review, *Postharvest biology and technology* 46 (2) (2007) 99–118.
- [5] H. Patel, R. Prajapati, M. Patel, Detection of quality in orange fruit image using svm classifier, in: ICQEI, IEEE, 2019, pp. 74–78.
- [6] P. Bergmann, M. Fauser, D. Sattlegger, C. Steger, Mvtec ad—a comprehensive real-world dataset for unsupervised anomaly detection, in: CVPR, IEEE, 2019, pp. 9592–9600.
- [7] N. Khalid, A. Abdullah, S. Shukor, F. S. AS, H. Mansor, N. Dalila, Non-destructive technique based on specific gravity for post-harvest mangifera indica l. cultivar maturity, in: AMS, IEEE, 2017, pp. 113–117.
- [8] K. Roy, S. S. Chaudhuri, S. Bhattacharjee, S. Manna, T. Chakraborty, Segmentation techniques for rotten fruit detection, in: Optronix, IEEE, 2019, pp. 1–4.
- [9] STELZNER, Fruit penetrometer, <https://pronova.de/en/products/agricultural-measuring/fruit-analysis/804>.
- [10] Jacks jk-100r penetrometer moisture analyzer, <https://www.chem17.com/product/detail/28186372.html>.
- [11] Yamato adp-31 vaccum oven, https://www.idealvac.com/files/brochures/yamatovacuumovenadp21_31.pdf.
- [12] Mileseey sm20 ssc analyzer, <http://www.mileseey.com/ProductCenter/ProductCenterList1034/>.
- [13] Atago pallete pr101 ssc analyzer, <https://www.instrument.com.cn/netshow/SH102225/C161297.htm>.
- [14] W. Jiang, G. Marini, N. van Berkel, Z. Sarsenbayeva, Z. Tan, C. Luo, X. He, T. Dingler, J. Goncalves, Y. Kawahara, et al., Probing sucrose contents in everyday drinks using miniaturized near-infrared spectroscopy scanners, *IMWUT* 3 (4) (2019) 1–25.
- [15] Asd labspec 4 hi-res analytical instrument, <https://www.malvernpanalytical.com/en/products/product-range/asd-range/labspec-range/labspec-4-hi-res-analytical-instrument>.
- [16] M. Ecartot, P. Bączyk, L. Tessarotto, C. Chervin, Rapid phenotyping of the tomato fruit model, micro-tom, with a portable vis-nir spectrometer, *Plant physiology and biochemistry* 70 (2013) 159–163.
- [17] R. Lu, Nondestructive measurement of firmness and soluble solids content for apple fruit using hyperspectral scattering images, *Sensing and Instrumentation for Food Quality and Safety* 1 (1) (2007) 19–27.
- [18] J. F. I. Nturambirwe, H. H. Nieuwoudt, W. J. Perold, U. L. Opara, Non-destructive measurement of internal quality of apple fruit by a contactless nir spectrometer with genetic algorithm model optimization, *Scientific African* 3 (2019) e00051.
- [19] Felix f-750, <https://felixinstruments.com/food-science-instruments/portable-nir-analyzers/f-750-produce-quality-meter/>.

- [20] A. Ren, A. Zahid, A. Zoha, S. A. Shah, M. A. Imran, A. Alomainy, Q. H. Abbasi, Machine learning driven approach towards the quality assessment of fresh fruits using non-invasive sensing, *IEEE Sensors Journal* 20 (4) (2019) 2075–2083.
- [21] S. Tan, L. Zhang, J. Yang, Sensing fruit ripeness using wireless signals, in: *ICCCN*, IEEE, 2018, pp. 1–9.
- [22] J. Ding, R. Chandra, Towards low cost soil sensing using wi-fi, in: *Mobicom*, ACM, 2019, pp. 1–16.
- [23] C. Feng, J. Xiong, L. Chang, J. Wang, X. Chen, D. Fang, Z. Tang, Wimi: Target material identification with commodity wi-fi devices, in: *ICDCS*, IEEE, 2019, pp. 700–710.
- [24] U. Ha, J. Leng, A. Khaddaj, F. Adib, Food and liquid sensing in practical environments using rfids, in: *NSDI*, USENIX, 2020, pp. 1083–1100.
- [25] B. Xie, J. Xiong, X. Chen, E. Chai, L. Li, Z. Tang, D. Fang, Tagtag: material sensing with commodity rfid, in: *Sensys*, ACM, 2019, pp. 338–350.
- [26] J. Wang, J. Xiong, X. Chen, H. Jiang, R. K. Balan, D. Fang, Tagscan: Simultaneous target imaging and material identification with commodity rfid devices, in: *Mobicom*, ACM, 2017, pp. 288–300.
- [27] A. Dhekne, M. Gowda, Y. Zhao, H. Hassanieh, R. R. Choudhury, Liquid: A wireless liquid identifier, in: *Mobisys*, ACM, 2018, pp. 442–454.
- [28] H.-S. Yeo, G. Flamich, P. Schrempf, D. Harris-Birtill, A. Quigley, Radarcat: Radar categorization for input & interaction, in: *UIST*, 2016, pp. 833–841.
- [29] Y. Zhu, Y. Zhu, B. Y. Zhao, H. Zheng, Reusing 60ghz radios for mobile radar imaging, in: *Mobicom*, ACM, 2015, pp. 103–116.
- [30] Y. Ren, S. Tan, L. Zhang, Z. Wang, Z. Wang, J. Yang, Liquid level sensing using commodity wifi in a smart home environment, *IMWUT* 4 (1) (2020) 1–30.
- [31] D. Wu, R. Gao, Y. Zeng, J. Liu, L. Wang, T. Gu, D. Zhang, Fingerdraw: Sub-wavelength level finger motion tracking with wifi signals, *IMWUT* 4 (1) (2020) 1–27.
- [32] Tpf 750 fruit spectrometer (portable), <http://www.top17.net/product/2873.html>.
- [33] ideaoptics nir1700 spectrometer, <http://www.ideaoptics.com/SucessCase/Ncontent.aspx?id=65509741-b5fb-491d-a204-7d9625d048cc>.
- [34] D. E. Khaled, N. Novas, J. A. Gazquez, R. M. Garcia, F. Manzano-Agugliaro, Fruit and vegetable quality assessment via dielectric sensing, *Sensors* 15 (7) (2015) 15363–15397.
- [35] D. Devices, Gs3 water content, ec, and temperature sensors operator’s manual, http://www.ictinternational.com/content/uploads/2014/03/13822_GS3_Web.pdf (2011).
- [36] Lenntech, Water conductivity, <https://www.lenntech.com/applications/ultrapure/conductivity/water-conductivity.htm>.
- [37] C. Wang, J. Liu, Y. Chen, H. Liu, Y. Wang, Towards in-baggage suspicious object detection using commodity wifi, in: *CNS*, IEEE, 2018, pp. 1–9.
- [38] A. S. D. W. D. H. Wenjun Hu, Linux 802.11n csi tool, <https://github.com/dhalperi/linux-80211n-csitool/>.
- [39] J. Gjengset, J. Xiong, G. McPhillips, K. Jamieson, Phaser: Enabling phased array signal processing on commodity wifi access points, in: *Mobicom*, ACM, 2014, pp. 153–164.
- [40] M. Kotaru, K. Joshi, D. Bharadia, S. Katti, Spotfi: Decimeter level localization using wifi, in: *Sigcomm*, 2015, pp. 269–282.
- [41] Y. Xie, Y. Zhang, J. C. Liando, M. Li, Swan: Stitched wi-fi antennas, in: *Mobicom*, 2018, pp. 51–66.
- [42] K. Niu, F. Zhang, Z. Chang, D. Zhang, A fresnel diffraction model based human respiration detection system using cots wi-fi devices, in: *UbiComp*, ACM, 2018, pp. 416–419.
- [43] Y. Xie, Z. Li, M. Li, Precise power delay profiling with commodity wi-fi, *IEEE Transactions on Mobile Computing* 18 (6) (2018) 1342–1355.
- [44] N. Yu, W. Wang, A. X. Liu, L. Kong, Qgesture: Quantifying gesture distance and direction with wifi signals, *IMWUT* 2 (1) (2018) 1–23.
- [45] H. Dang, J. Song, Q. Guo, A fruit size detecting and grading system based on image processing, in: *IHMSC*, Vol. 2, 2010, pp. 83–86.
- [46] Y. Zhang, Z. Dong, X. Chen, W. Jia, S. Du, K. Muhammad, S. Wang, Image based fruit category classification by 13-layer deep convolutional neural network and data augmentation, *Multim. Tools Appl.* 78 (3) (2019) 3613–3632.
- [47] W.-c. Guo, S. O. Nelson, S. Trabelsi, S. J. Kays, 10–1800-mhz dielectric properties of fresh apples during storage, *Journal of Food engineering* 83 (4) (2007) 562–569.
- [48] W. Guo, X. Zhu, S. O. Nelson, R. Yue, H. Liu, Y. Liu, Maturity effects on dielectric properties of apples from 10 to 4500 mhz, *LWT-Food Science and Technology* 44 (1) (2011) 224–230.
- [49] D. Xie, D. Liu, W. Guo, Relationship of the optical properties with soluble solids content and moisture content of strawberry during ripening, *Postharvest Biology and Technology* 179 (2021) 111569.
- [50] J. A. Hartigan, M. A. Wong, Algorithm as 136: A k-means clustering algorithm, *Journal of the royal statistical society. series c (applied statistics)* 28 (1) (1979) 100–108.
- [51] G. Guo, H. Wang, D. Bell, Y. Bi, K. Greer, Knn model-based approach in classification, in: *OTM Confederated International Conferences” On the Move to Meaningful Internet Systems”*, Springer, 2003, pp. 986–996.
- [52] N. Muramatsu, N. Sakurai, N. Wada, R. Yamamoto, K. Tanaka, T. Asakura, Y. Ishikawa-Takano, D. J. Nevins, Remote sensing of fruit textural changes with a laser doppler vibrometer, *Journal of the American Society for Horticultural Science* 125 (1) (2000) 120–127.
- [53] H. Matsui, T. Hashizume, K. Yatani, Al-light: An alcohol-sensing smart ice cube, *IMWUT* 2 (3) (2018) 1–20.
- [54] S. Lee, B.-K. Cho, Evaluation of the firmness measurement of fruit by using a non-contact ultrasonic technique, in: *ICIEA*, IEEE, 2013, pp. 1331–1336.

- [55] F. YILDIZ, A. T. ÖZDEMİR, S. ULUIŞIK, Custom design fruit quality evaluation system with non-destructive testing (ndt) techniques, in: IDAP, IEEE, 2018, pp. 1–5.
- [56] Cisco annual internet report (2018–2023) white paper, <https://www.cisco.com/c/en/us/solutions/collateral/executive-perspectives/annual-internet-report/white-paper-c11-741490.html> (Mar. 2020).
- [57] M. M. Atia, A. Noureldin, M. J. Korenberg, Dynamic online-calibrated radio maps for indoor positioning in wireless local area networks, *IEEE Transactions on Mobile Computing* 12 (9) (2012) 1774–1787.
- [58] N. Kviklienė, A. Valiuškaitė, P. Viškėlis, et al., Effect of harvest maturity on quality and storage ability of apple cv.'ligol', *Sodininkystė ir Daržininkystė* 27 (2) (2008) 339–346.